Fractals under the Microscope

or

Reaching Beyond
the Dimensional Formalism of Fractals
with the Wavelet Transform

Zbigniew R. Struzik

CWI, Kruislaan 413, 1098 SJ Amsterdam

The Netherlands

e-mail: zbyszek@cwi.nl

Recently, there has been a tendency to see natural phenomena as resulting from the action of dynamical processes. These processes (and the objects to which they give rise) are surprisingly often well characterised using some sort of hierarchical approach.

It is also one of the key features of fractal geometry that the action of dynamical systems can result in intrinsically hierarchical structures. In this paper we shortly outline the rapid progress which was made in analysis of fractals with the wavelet transform (often, but not exclusively, making use of the derivatives of the Gaussian kernel).

We demonstrate that the natural ability of the wavelet transform to analyse objects using both position and scale localised filters proves ideal in the context of hierarchical formalism of fractal geometry. In addition to this, the inherent robustness of the transform provides reliable access to multi-scale representations.

1. INTRODUCTION

Just a selection of the titles of monographs or collected works: *The Fractal Geometry of Nature* [1], *Fractals Everywhere* [2], *Fractal Reviews in the Natural and Applied Sciences* [3], would quickly give the reader an idea of the universality of the concept of fractal geometry. Going through the subjects of these books would confirm this impression. Indeed, fractals are found just

about everywhere in natural phenomena, problems in engineering sciences, or in works of art. Having realised this fact, one would expect that clear and reliable recipes exist for the purpose of isolating and characterising fractals. Unfortunately, in practical cases, the task of proving that the particular object at hand is fractal, with the tools available, is to say the least unreliable.

Still, the intuition of common sense perception of fractals would indicate something very different - it is enough to perform a simple experiment of breaking off the smaller and smaller branches from the broccoli bought in the nearby greengrocer to get the feeling of the primary characteristic of its parts *or* fractions. In case observations become difficult one might use a magnifying glass, ideally bringing the size of the magnified branch to that of the original broccoli. While we encourage the reader to convince himself, let us just point out that the magnified branches would be very similar to the original broccoli, and this feature, called *self-similarity*, turns out to be universal for fractal objects.

This is also the notion which, in all practical terms, loosely defines the fractal, in spite of the existence of a variety of more or less advanced criteria which generally can be referred to as *fractal dimensions*. Without going into details, the dimensional characterisation of fractals although definitely of great value, has one major shortcoming - it remains global in its very nature and assigns, not always reliably, the object in question to some universality class.

Even though an admittedly complex structure, the broccoli in our experiment is undoubtedly neither random, nor is it exactly self-similar. Yet the dimensional characterisation would fail to distinguish it from these extremal cases. Under successive magnifications, the complex structure appears to consistently follow some principle, within the rather obvious finite size bounds of flower resolution and the broccoli size. This thought is the key idea of the work we shortly report here - there must be some *construction rule* apparently hidden in the complex structure of a fractal. It can vary from completely deterministic to completely random, still we propose that it is there!

This is also the problem formulation posed in the thesis work [4]. The methodology we developed there is supposed to provide answers to the *existence of a fractal* problem through the recovery of the original construction rule or its main characteristics. In its essence going to the very fundamental way of looking at fractal objects, the main tool used to make this proposition plausible is similar to that we used in our broccoli experiment - the *mathematical microscope* - this is how the Continuous Wavelet Transform (CWT) was first referred to in the context of fractal analysis [5].

We employed it to perform the analysis of some example fractal structures, which we introduce in Section 2 of this work, and reveal their consistent scaling behaviour - renormalisation structure, leading in turn to the construction rule recovery. This approach is shown to extend the available dimensional characterisation of fractals outlined in Section 3.

We introduce the CWT in Section 4, first shortly showing how it proved to be particulary useful in local characterisation of singular detail essentially contributing to a fractal's shape. But more interestingly for our purpose, the

property of inheriting the renormalisation properties of the invariant fractal object by the wavelet transform is next used to build a bifurcation-based WTMB representation representing the information on the scale-position localised (invariant) grid, allowing tracing the actions of the renormalisation group in the wavelet decomposition.

The major feature of this approach, outlined further in Section 4, is the possibility of verifying such a scale-space similarity in terms of invariance with respect to some iterative functions (maps). Contrary to the methods known from the field of fractal compression of images, which use a predefined class of Iterated Function System functions [2] to approximate the invariance in question, the approach we present aims at revealing the renormalisation involved in the creation of the fractal, possibly bearing relevance to the underlying physical phenomena.

Our hypothesis is therefore, that an object can be classified as a pre-fractal if there exists a solution to the related inverse fractal problem; in other words, if a set of construction rules can be found, which would define main (scaling) characteristics of the object. Ultimately, the construction rule can, of course, be expected to fully define the object within the scales where it is observed and which allows arbitrary extrapolation in the scale domain.

As already mentioned, solving the inverse fractal problem for self-affine functions is done by means of testing the invariance of the wavelet transform modulus maxima representation of the function. For this purpose, several algorithm designs are possible. The most reliable and powerful approach to date, which we will also describe in some detail in Section 4, uses the topological structure of the maxima lines and characteristic invariant points like bifurcations, inherently present in the wavelet transform in the form of relating bifurcations to the maxima lines. [1] This data-structure rather than a model driven approach is, therefore, able to recover non-linear maps by its very virtue of not being bound to a particular model.

Two and three dimensional fractals occur frequently in the real world, and parameterization or cuts reducing dimensionality but retaining the fractal aspects of the object are not always straightforward or even possible. The extension to an intrinsically two dimensional analysis of fractals on one- to two-dimensional support (embedded in 2D) is shortly discussed in Section 5.

2. VARIETY OF FRACTAL TYPES

2.1. Some well-known fractal sets

We will begin with the von Koch curve, perhaps the most familiar example of fractal construction. It can be created by dividing a line segment L (constituting the so-called initiator, $L \equiv F_0$) into three equal parts and then replacing the middle one with two identical ones, which are joined to form an equilateral triangle without a base, which fits precisely in the space left by the one removed. The *generator* made in this way is next scaled by a factor $1/3$ and used

---

[1] A tree-matching technique for recovering maps was also developed by Arneodo et al. [6]

111

recursively to replace each of the line segments of the previous *construction stage*. See Figure 1. The procedure can be carried on indefinitely, resulting in an object, the so-called *attractor* set with somewhat strange properties: even though the von Koch attractor is a curve, it has an infinite length in the limit, as a simple calculation can show. On the other hand, its area in the plane is zero, thus neither length nor area provide a useful measure of it. Moreover, it is nowhere differentiable in the sense that one cannot define tangents to it at any point.
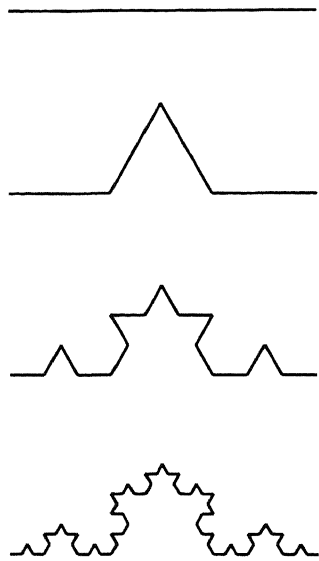
FIGURE 1. The first four stages of generation (F_i, $i = 0 \ldots 3$) of the von Koch curve. The von Koch island or snowflake is also shown.

Somewhat less attractive in appearance and probably the simplest fractal structure, our next example is the middle third Cantor set. Nevertheless, it can be generalised to one of the theoretically most important class of fractals as we will demonstrate in the following Subsection 2.3. The construction proceeds as follows: from the line segment $L \equiv F_0$ divided into three equal parts, we remove the middle third. This action is next performed on the remaining parts. The result of this action of middle third removal to infinity, in the limit does, however, leave *some* fractal 'dust', the Cantor set; see Figure 2.

The Sierpiński triangle, yet another well-known example, has in its construction much in common with the Cantor set except that its creation happens in two dimensions resulting in a generic 2D fractal. It can be obtained by repeatedly removing triangles from the initial filled triangle, as is demonstrated in
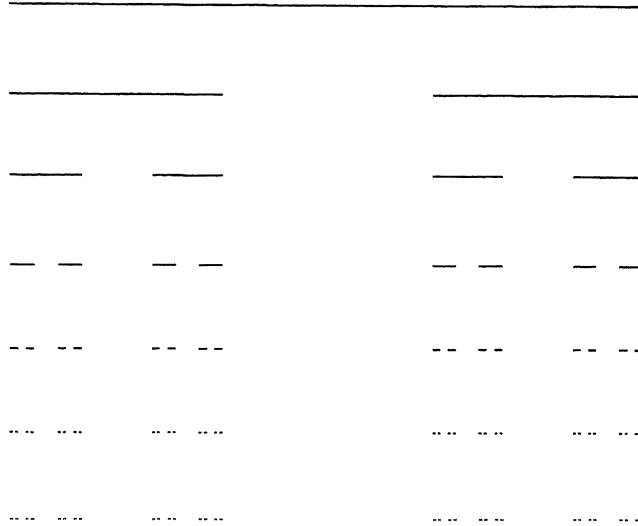
FIGURE 2. Starting from the line segment F_0, five generation steps of the Cantor set follow, up to F_6.

Figure 3. The same Sierpiński triangle will be obtained if the initial object is a square which is next divided into four equal squares of which one (e.g. bottom right) is removed, see Figure 4. This is not a rare duality of Sierpiński construction, but a universal property behind the fractal (attractor) construction. It is the transformations of similarity, expressed in the idea of the generator and containing the scaling and translating transformations which fully define the resulting object.

Indeed, recursively repeating the similarity transformations to infinity results in the fractal object, provided the transformations contract space (notice that the rescaling factor is always less than one). The shape of the initial object used to 'feed' the generator is not so important;[2] all initially distant points will be 'squeezed' by the contracting similitudes into the limit fractal shape, which for this reason is also called the *fractal attractor*.

The construction process for each of the examples introduced can, therefore, be fully described by a set of *rules* involving the transformations of similarity. In the Cantor set case, these will be only two transformations (similitudes) acting on the line:

1. S_{1_C} - scale by 1/3 and place at $x' = 0 \; x$;

2. S_{2_C} - scale the 1/3 and place at $x' = 2/3 \; x$.
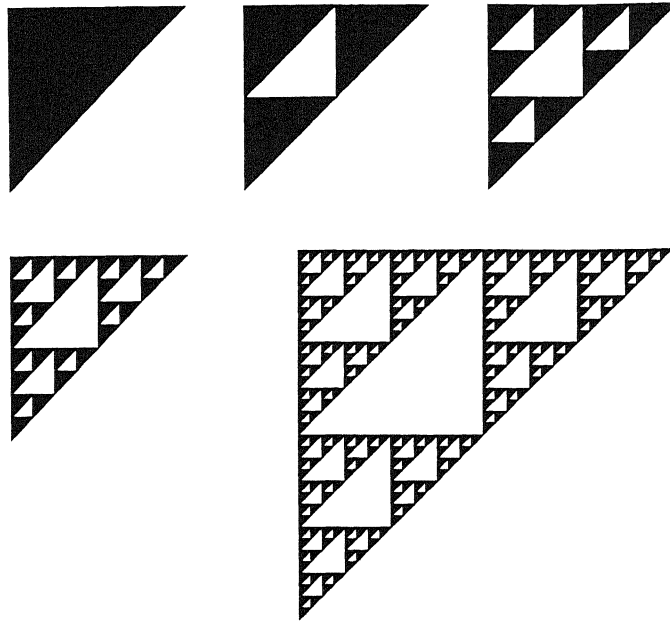
---

[2] it has to be a compact set

FIGURE 3. The Sierpiński triangle: From a filled triangle F_0, an inverted triangle is removed in the first generation step to give F_1. The three remaining, still filled triangles are next subject to the same transformation of inverted triangle removal to give F_2. The followings generations are shown, F_0 through F_3 and twice enlarged F_5.

For the Sierpiński triangle, the transformations will be three affine transformations in the plane $\{X, Y\}$:

1. S_{1_S} - scale by 1/2 (along x and y) and translate by $x' = 0\,x$, $y' = 0\,y$;

2. S_{2_S} - scale by 1/2 and translate by $x' = 1/2\,x$, $y' = 0\,y$;

3. S_{3_S} - scale by 1/2 and translate by $x' = 0\,x$, $y' = 1/2\,y$.

And for our first fractal example, the von Koch curve, we need four transformations:

1. S_{1_K} - scale by 1/3 (along x and y) and translate by $x' = 0\,x$, $y' = 0\,y$;

2. S_{2_K} - scale by 1/3, rotate by $\pi/6$ and translate by $x' = 1/3\,x$, $y' = 0\,y$;

3. S_{3_K} - scale by 1/3, rotate by $\pi/6$ and transl. by $x' = 1/2\,x, y' = \sqrt{(3)}/2y$;

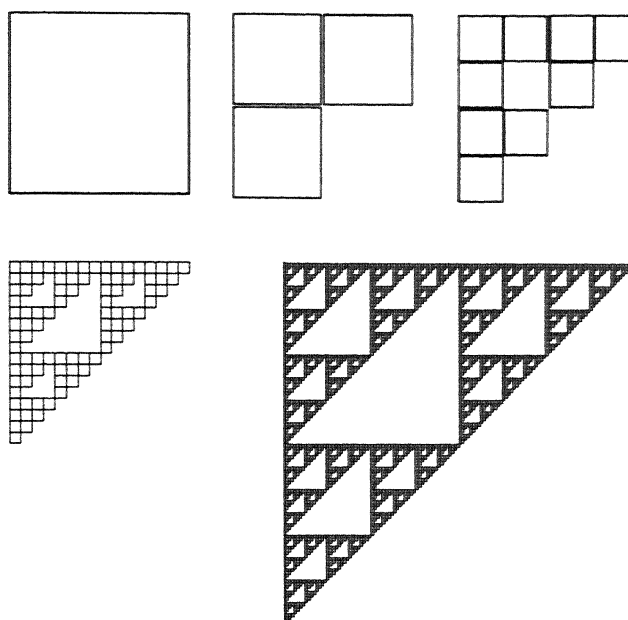4. S_{4_K} - scale by 1/3 and translate by $x' = 2/3\,x$, $y' = 0\,y$.

114

FIGURE 4. The Sierpiński triangle: starting from a perimeter of a square F_0, the two first generation steps F_1 and F_2 are shown, followed by F_4 and twice enlarged F_7.

2.2. Self-similarity and self-affinity

As is to be expected, the above rules defining the well-known examples introduced can be represented in a somewhat more appropriate flexible general formalism. It represents the set of construction actions as parameterizable similitudes which can be used to generate a variety of fractals. The central formal concept here is that of the *affine transformation* or an *affinity*, which we will call a mapping $S : \mathbb{R}^n \rightarrow \mathbb{R}^n$ of the form:

$$S(x) = T(x) + b,$$

where T is a non-singular linear transformation on $\mathbb{R}^n$ (often represented by an $n \times n$ matrix) and b is a vector in $\mathbb{R}^n$.

Generally, an affinity is a shearing transformation; its contracting or expanding effect do not need to be the same in all directions. For our considerations we will allow only such transformations S which have the *contracting* property, which is saitisfied if there is a number c with $0 < c < 1$, such that $|S(x) - S(y)| \leq c|x - y|$ for all x, y in $\mathbb{R}^n$. Such a transformation $S : \mathbb{R}^n \rightarrow \mathbb{R}^n$ is then called a contraction and it still has the freedom to contract with differing ratios in different directions. As a special case constituting an important class, we have (contracting) *similarities* contracting isotropically: if $|S(x) - S(y)| = c|x - y|$ for all x, y in $\mathbb{R}^n$ then S is a similarity.

All the examples shown so far used similarity transformations. Let us demonstrate how the presented examples fit in this formalism. The Cantor set construction can be simply described by two one-dimensional transformations:

$$x'^{s_1} = S_1(x) = (1/3)(x) + (1/3)(0) ;$$
$$x'^{s_2} = S_2(x) = (1/3)(x) + (1/3)(2) . \qquad (1)$$

The matrix notation of the transformation leading to the Sierpiński triangle is similarly defined with respect to (x, y) coordinates:

$$S_1 \begin{pmatrix} x \\ y \end{pmatrix} = \begin{pmatrix} 1/2 & 0 \\ 0 & 1/2 \end{pmatrix} \begin{pmatrix} x \\ y \end{pmatrix} + \begin{pmatrix} 0 \\ 0 \end{pmatrix} ;$$

$$S_2 \begin{pmatrix} x \\ y \end{pmatrix} = \begin{pmatrix} 1/2 & 0 \\ 0 & 1/2 \end{pmatrix} \begin{pmatrix} x \\ y \end{pmatrix} + \begin{pmatrix} 1/2 \\ 0 \end{pmatrix} ;$$

$$S_3 \begin{pmatrix} x \\ y \end{pmatrix} = \begin{pmatrix} 1/2 & 0 \\ 0 & 1/2 \end{pmatrix} \begin{pmatrix} x \\ y \end{pmatrix} + \begin{pmatrix} 0 \\ 1/2 \end{pmatrix} . \qquad (2)$$

The von Koch curve is best represented by a set of four transformations in the plane,[3] for which the matrix notation is:

$$S_1 \begin{pmatrix} x \\ y \end{pmatrix} = \begin{pmatrix} 1/3 & 0 \\ 0 & 1/3 \end{pmatrix} \begin{pmatrix} x \\ y \end{pmatrix} + \begin{pmatrix} 0 \\ 0 \end{pmatrix} ;$$

$$S_2 \begin{pmatrix} x \\ y \end{pmatrix} = \begin{pmatrix} 1/2 & -\sqrt{(3)}/2 \\ \sqrt{(3)}/2 & 1/2 \end{pmatrix} \begin{pmatrix} 1/3 & 0 \\ 0 & 1/3 \end{pmatrix} \begin{pmatrix} x \\ y \end{pmatrix} + \begin{pmatrix} 1/3 \\ 0 \end{pmatrix} ;$$

$$S_3 \begin{pmatrix} x \\ y \end{pmatrix} = \begin{pmatrix} 1/2 & \sqrt{(3)}/2 \\ -\sqrt{(3)}/2 & 1/2 \end{pmatrix} \begin{pmatrix} 1/3 & 0 \\ 0 & 1/3 \end{pmatrix} \begin{pmatrix} x \\ y \end{pmatrix} + \begin{pmatrix} 1/2 \\ \sqrt{(3)}/2 \end{pmatrix} ;$$

$$S_4 \begin{pmatrix} x \\ y \end{pmatrix} = \begin{pmatrix} 1/3 & 0 \\ 0 & 1/3 \end{pmatrix} \begin{pmatrix} x \\ y \end{pmatrix} + \begin{pmatrix} 2/3 \\ 0 \end{pmatrix} . \qquad (3)$$

Our first fractal example again requires not only the highest number of similitudes, their form is also slightly more complicated since it includes rotations. We indicated this by writing separately the rotation and dilation transformation.

Suppose we apply the transformations Equation (1) to generate the Cantor set. After the first generation we have $\{S_1(F_0), S_2(F_0)\}$. The second action leads to $\{S_1 \circ S_1, S_1 \circ S_2, S_2 \circ S_1, S_2 \circ S_2\}$, where we neglected indicating the initial object F_0, and denoted the transformation of composition of transformations S_i with $\circ$. The effective contraction rate of each of these four combinations of transformations in the second stage of generation is, of course, $1/3 \; 1/3 = 1/9$. Moreover, each combination defines uniquely the resulting 'object' - $S_i \circ S_j(F_0)$, $i, j \in \{1, 2\}$.

---

[3] Since it is generically a curve, the von Koch construction can be also parameterized to give one-dimensional function.

This means each object is also designated an unique combination of indexes $\{(1,1),(1,2),(2,1),(2,2)\}$. Had we used numbering starting from zero for indexing the similitudes, we would have recovered a unique *binary address* of each element of the Cantor set, respectively $00, 01, 10, 11$. The third generation adds the rightmost (least meaningful) bit, and so on... Similar consideration for the Sierpiński triangle would lead to unique triadic addresses, and for the von Koch curve, quadric. These sequences of transformations will also be referred to as the *kneading sequences* the terminology which stems from the theory of chaotic dynamical systems.

Repetitively applying the set of contraction transformations $S_n, n = 1 \ldots N$ to infinity does not, perhaps surprisingly, lead to the vanishing of the fractal shape. We have already shown some examples of the limit shapes of example constructions, the so-called (fractal) attractors. Indeed, each element of the attractor can still be identified by its, now infinitely long, address.

For the rigorous proof of this conjecture see, for example [10]. By this standard result, if $S_1, \ldots, S_N$ are affine contractions on $\mathbb{R}^n$, the unique compact set F invariant with respect to S_n is guaranteed to exist and is termed a *self-affine set* or an *attractor* of $S_n, n = 1, \ldots, N$.

Therefore, the following *invariance* relation is satisfied:

$$F = \bigcup_{n=1}^{N} S_n(F) \tag{4}$$

for the self-affine set F obtained by

$$F_k = \left[\bigcup_{n=1}^{N} S_n \right]^{\circ k}(B) \qquad \text{for any } B \subset \mathbb{R}^n ; \qquad F = \lim_{k \to \infty} F_k , \tag{5}$$

where $\circ$ denotes the composition of contractions, so that

$$(P_1 \circ P_2 \circ \ldots \circ P_k)(x) = P_1(P_2(\ldots(P_k(x))\ldots)).$$

If F is a fractal, the subsequent approximations F_k of the set F will be called *pre-fractals*.

In the following we will restrict ourselves to non-overlapping transformations that is such that the union in (4) is disjoint or they do not overlap 'too much'. For this we will require the components S_i to satisfy an *open set condition*; i.e. there must exist a non-empty bounded open set V such that $V \supset \bigcup_{n=1}^{N} S_n(V)$ with the union disjoint.

Naturally, in the case where the set satisfies the invariance relation (4), in which all the transformations S_n are similarities, the set F is called *self-similar*. Whether self-similar or self-affine, the fractals defined so far can generally be described as sets. The applicability of the concept of set is, however, somehow restricted in the natural sciences. Observables from the real world are often more appropriately represented as (fractal) functions or measures like probability distributions, all possessing an intrinsic independently scaling *density*

component. Such measures and functions, which also need to account for distributions (and this *generalisation* we will take by default), will often - but not necessarily be defined on fractal support.

2.3. Fractal functions (IFP formulation)

Generally speaking there is no restrictions on the class of functions which graphs can posess fractal properties. Both continuous mappings and tempered distributions include fractal examples. Time series, from medicine, technology or economics, density distributions in geology, astronomy or physics provide an unlimited source of potentially fractal functions. We have already seen how the affine transformation can be used to construct sets, let us in the following demonstrate how the concept of the fractal function or measure distribution is intimately related to the affine transformation and self-affinity. We will consider the continuous contraction transformations $S_i : \mathbb{R}^2 \to \mathbb{R}^2$, $i = 1, \ldots, N$, in short to be called *maps*, like those defined in the previous subsection.

The crucial extension to the formalism of fractal sets was the introduction of the measure's (mass) density component, the scaling of which is independent of the scaling of its support. In particular, this generalisation over measures following multiplicative scaling rules, gave rise to the extension of the fractal formalism of sets over the *multi-fractal* formalism.

The first construction to be introduced, the so-called Besicovitch measure, has become practically a standard illustration of the concept in works treating the multi-fractal formalism. Not without importance here is the fact that it remains one of the few analytically tractable examples of multi-fractals. Nevertheless, although conceptually simple, the Besicovitch measure example can be considered fundamental to many physical phenomena.

The Besicovitch measure is actually a simple extension to the previously introduced Cantor set through equipping it with multiplicative measure. At each generation step the normalised measure is being consistently transferred with some fixed *repartition* ratio over the elements of the set constituting the current generation. It is easy to check that each step of generation increases the density of the measure by the factor 3/2, while the total measure remains constant.

Beyond this homogeneous and uniform case, there is a possibility of generalising this construction through non-equal factors defining non-uniform, multiplicative repartitioning of the measure. To do this, one again takes a unit measure and distributes it with the arbitrary ratios p_1 and p_2 over the two remaining sections of the line at each construction step. Naturally, the ratios $c_1^{-1} = c_2^{-1} = 1/3$ defining the middle-third Cantor set can as well be set to non-uniform. Also, the number of divisions, which is equivalent to the number of transformations, see (1), can be subject to alteration (increase).

The set of transformations describing the Besicovitch construction can be expressed as:
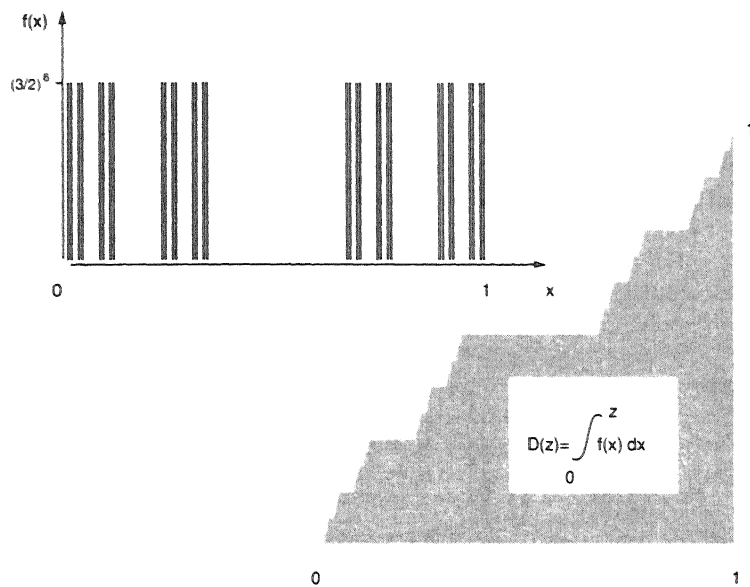
FIGURE 5. The triadic Cantor measure, generation F_6, and the devil's staircase created by integrating the Cantor measure.

$$f'^{B_1}(x) = B_1 \, f(x) = p_1 \, f(\frac{x + b_1}{c_1}) \; ;$$

$$f'^{B_2}(x) = B_2 \, f(x) = p_2 \, f(\frac{x + b_2}{c_2}) \; , \qquad (6)$$

with the normalisation requirement

$$p_1 + p_2 = 1 \; . \qquad (7)$$

Additionally, we put conditions ensuring non-overlapping of the transformations:

$$\frac{1 + b_1}{c_1} < \frac{0 + b_2}{c_2}$$

while all the respective values $b_1/c_1, b_2/c_2, c_1^{-1}, c_2^{-1}$ are from the interval $(0, 1)$.

For equal ratios, $p_1 = p_2 = 1/2$ and $c_1 = c_2 = 3$ with $b_1 = 0$ and $b_2 = 2$ we recover the middle-third, homogeneous distribution of measure on the Cantor set (Cantor generalised function). It can be integrated to give a related fractal object: the *devil's staircase*, see Figure 5. For non-equal p_i the resulting
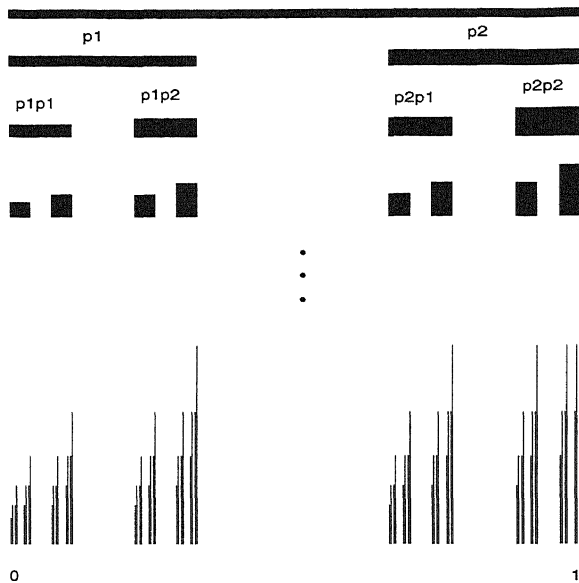
FIGURE 6. The Besicovitch measure on the Cantor set, generations F_0 through F_3 and the generation F_6. Distribution of weights is $P_1 = 0.4$ and $P_2 = 0.6$. The standard middle third Cantor division is retained.

multiplicative distribution of the measure constitutes the classical example of multi-fractal object, an example of which is given in Figure 6.

A straightforward extension to this concept of measure distribution is the slightly more involved construction of a self-affine function. Ironically, despite the simplicity of their construction, *general* self-affine functions proved to be relatively difficult to analyse in terms of fractal geometry. Leaving the aspects of fractal analysis to the next section, we would like to discuss a scheme of generation of this, our last example of a deterministic fractal function. It is a generalisation of the above introduced self-affine fractal construction involving intrinsically two-dimensional components in the affine transformation, and resulting in a genuine fractal function.

Suppose we place on the set of similitudes the requirement that the fractal attractor they define constitutes a functional mapping $f : \mathbb{R} \to \mathbb{R}$. This is easily achieved by imposing the following constraints on the similitudes S_n:
Let S_n $(1 \leq n \leq N)$ be affine transformations, represented in matrix notation with respect to (x, y) coordinates by

$$ S_n \begin{pmatrix} x \\ y \end{pmatrix} = \begin{pmatrix} \sigma_n^{-1} & 0 \\ \gamma_n & \alpha_n \end{pmatrix} \begin{pmatrix} x \\ y \end{pmatrix} + \begin{pmatrix} (n-1)\,\sigma_n^{-1} \\ \delta_n \end{pmatrix} . $$

Next, let $t_0 = (0, \delta_1/(1 - \alpha_1))$ and $t_N = (1, (\delta_N + \gamma_N)/(1 - \alpha_N))$ be the *fixed points* of S_1 and S_N (i.e. such that $S(t) = t$). We assume that the matrix

120

coefficients have been chosen so that

$$S_n(t_N) = S_{n+1}(t_1) \qquad\qquad 1 \leq n \leq N - 1 \,,$$

in order to ensure that the segments $[S_n(t_0),\ S_n(t_N)]$ join up to form an (open) polygon E_1. The invariant set F of the S_n can be constructed, at each generation step k, by recursively replacing line segments $\left[[S_n]^{\circ k}(t_0), [S_n]^{\circ k}(t_N)\right]$ by affine images of E_1.
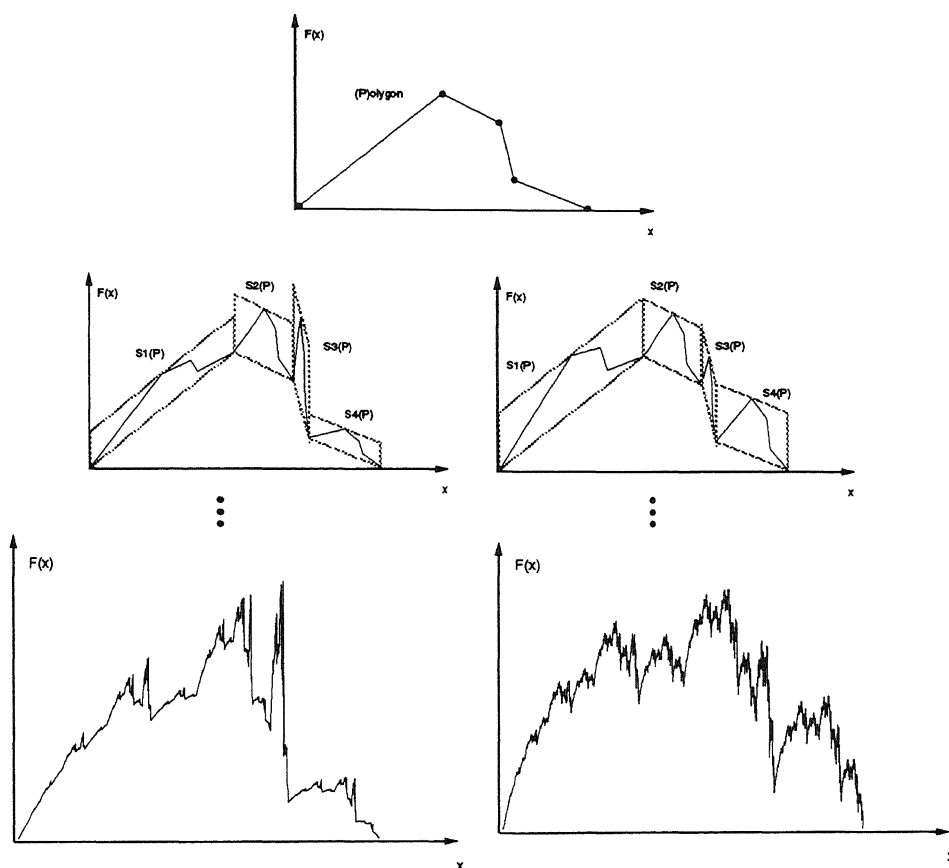

FIGURE 7. The initial set of data points F_0, interpolated using the self-affine construction. In the middle figures two cases of F_1, in the left for different values of the vertical scaling free parameter α_n, and in the right for the same $\alpha_n = 0.5$, for all $n = 1 \ldots 4$. Right below the plots of the (F_7) of the corresponding self-affine attractors.

The above scheme of generation of a self-affine attractor is often referred to as a fractal interpolation scheme (IFS)[2]. Indeed, the initial set of points
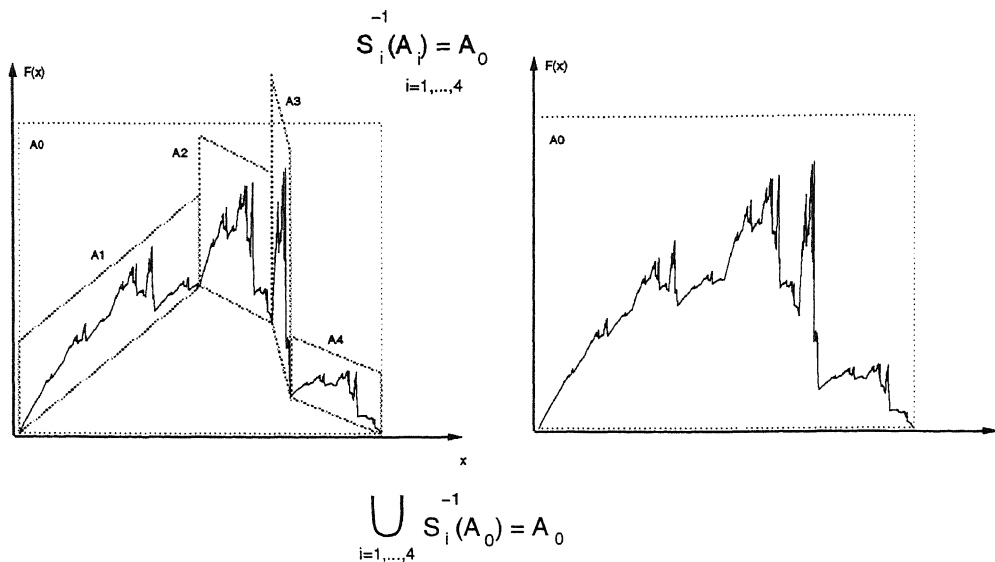
$$S_i^{-1}(A_i) = A_0$$

$$i = 1, \ldots, 4$$

$$\bigcup_{i=1,\ldots,4} S_i^{-1}(A_0) = A_0$$

FIGURE 8. The self-affine attractor is invariant with respect to the operators $S_n, 1 \ldots n$ used to construct the attractor.

t_i, $i = 0 \ldots N$, is interpolated by the attractor F according to the 'construction rule' implicitly contained in this set.

An example of a self-affine function with four maps, to which reference is made in the following part of this work, is shown in Figure 7 (right). The majority of parameters implied through the data set $\{t_i\}, i = 0, \ldots, N$, the vertical, in the y direction, scaling $\alpha_n, n = 1, \ldots, N$ remain free. The influence of this scaling factor on the form of the attractor is demonstrated for two cases; in the left branch of Figure 7, the attractor is created for several different values of α_n, while in the right branch α_n is chosen to be the same for all the affine transformations. The infinitely developed fractal attractor is invariant with respect to the affine transformations $S_n, n = 1, \ldots, 4$, see Figure 8.

3. STANDARD WAYS OF CHARACTERISING FRACTALS

3.1. Fractal dimension(s) of sets

We have already pointed out that classical geometry concepts are not suited to characterising fractal shapes: the von Koch curve is neither a line in strict sense nor does it fill the plane, the Cantor dust an invisible part of straight line but still it exists. [1] The main tool which proved useful in characterising fractal objects is the dimension in many forms, starting from similarity dimension used for illustrative purposes, through the Hausdorff dimension - a strictly

---

[1] This of course applies to the infinitely developed fractals, not to pre-fractals!

mathematically oriented tool, to the box dimension, the concept thus far most widely used practically.

Let us use the concept of similarity as the starting point in defining a way of characterising fractal objects and introduce the potentially *fractional* similarity dimension. Many fractals exhibit some sort of similarity – they contain parts which are similar to the complete object in some way. By similarity, we can, for a start, mean the concept traditionally defined in geometry. Two geometrical objects would be similar if, in result of uniform rescaling (and perhaps translation), one could resolve identity between them. In this way a piece of straight line is similar to its one-third part by the factor three, and one-fourth part of a filled square would have to be rescaled by the factor two to revert to the original.

It is a matter of course that the scaling (*renormalising*) ratios used to relate the complete object to its parts are somehow related to the dimension of the objects. Indeed, in the case of a line segment, it can be split in, for example, three equal parts, each constituting 1/3 of the original. Similarly, in the case of the rectangle, if divided in four identical rectangles, each part would be a copy of the original by the factor 1/2. If the *similarity* dimension is defined as the *rate of filling the embedding space*:

$$D_{sim(ilarity)} = -\frac{\log(\text{number of subparts of the object})}{\log(\text{scaling factor})}$$

we immediately recover $D_{sim} = -\log(3)/\log(1/3) = 1$ for the piece of line, and $D_{sim} = -\log(4)/\log(1/2) = 2$ for the square piece of plane.

The intuitive feeling of the dimension would tell us that for the examples introduced in the previous section, the dimension of the von Koch curve should be somewhere between $D_{line} = 1$ and $D_{plane} = 2$, that is the dimensions of line and plane respectively. For the Cantor set, it should be found somewhere between $D_{point} = 0$ and $D_{line} = 1$, which are the topological dimensions of point and line. In order to give a quantitative measure to the intuition outlined above, let us analyse the rate at which the example fractals fill their embedding dimensions.

Again, this can be observed by comparing the scaling characteristic to the self-similar components of the fractal to the corresponding scaling of the embedding space. In the case of the von Koch curve, the total shape can be divided into four similar parts. Each of these parts is, however, a 1/3 size copy of the original shape, thus the rate of filling the embedding 2D plane can be expressed with $D_{sim} = -\log(4)/\log(1/3) = 1.2619\ldots$. The middle third Cantor set can be analysed in a similar way. At each construction stage, there are two copies of the original scaled by 1/3 factor. Thus for the Cantor set $D_{sim} = -\log(2)/\log(1/3) = 0.6309\ldots$. As expected this number lies between $D_{point} = 0$ and $D_{line} = 1$.

The scope of such a characterisation is, however, limited to the class of strictly self-similar fractal sets, (hence we denote the dimension so obtained as
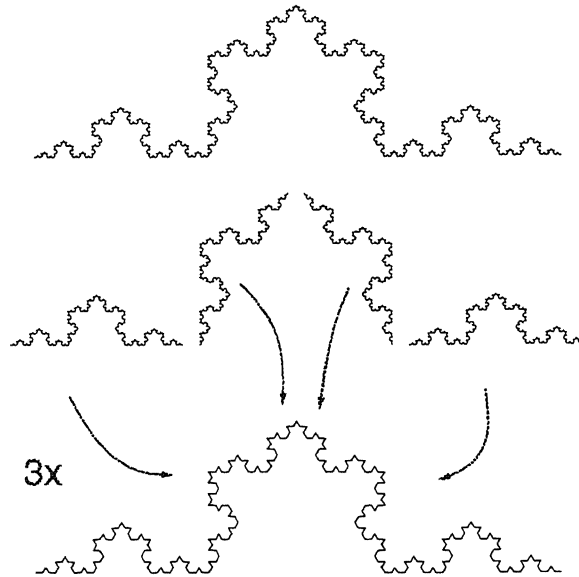
FIGURE 9. Calculating similarity dimension. Notice that due to the finite generation depth of the original, the rescaled parts are quasi-similar.

D_{sim}). Universally applicable concepts of dimension are the Hausdorff dimension and box counting dimension in its many variations.

Fundamental to these definitions of dimension is the idea of 'measurement at scale ϵ'. For each particular ϵ, we measure a set in a way that ignores detail of size less than ϵ, and while gradually changing ϵ, we observe how the measurements behave as $\epsilon \to 0$.

Let us define the so-called ϵ-covering of the set F, used to perform the measurement at scale ϵ, as

$$\mathcal{H}_\epsilon^s(F) = \inf \left\{ \sum_{i=1}^{\infty} |U_i|^s : \{U_i\} \text{ is an } \epsilon \text{ cover of } F \right\};$$

that is as the covering for which the sum of the s-th powers of the diameters of covering balls U_i is minimal (inf stands for infimum). For the collection $\{U_i\}$ to be $\epsilon - cover$ of F, it must be countable (of finite) and of diameter at most ϵ and, of course, it must contain F, i.e. $F \subset \bigcup_{n=1}^{N} U_n$. The limit value $\mathcal{H}^s(F)$ is called the s-dimensional Hausdorff measure of F:

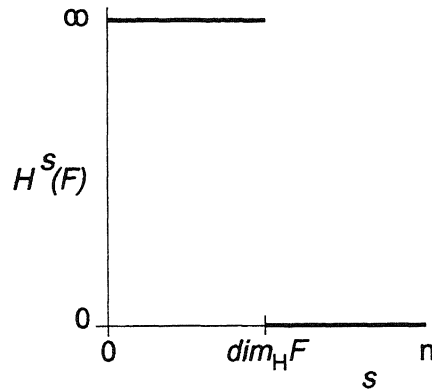$$\mathcal{H}^s(F) = \lim_{\epsilon \to 0} \mathcal{H}_\epsilon^s(F).$$

FIGURE 10. The Hausdorff dimension is the value of s for which the jump of Hausdorff measure takes place.

For most values of the parameter s, the Hausdorff measure equals 0 or ∞. There is, however, a critical value of s for which the jump occurs between these two values (which can easily be verified for the case when F is a non-fractal set). This value of the parameter s is referred to as the *Hausdorff dimension*.

While a perfectly good mathematical tool, this dimension is completely unsuitable for experimental purposes. Conveniently, there exists a commonly used alternative definition which is readily suitable for implementing on digital computers. With its many names (e.g. Kolmogorov entropy, entropy dimension, capacity dimension [10]), it is, however, best referred to as box or box counting dimension.

In its equivalent formulations, which differ in the way the ϵ-cover by means of boxes is performed, the box dimension is defined as the common value of the lower and upper *bounds* on the box counting dimension in the case that these are equal (FALCONER [10]). [2] Denoting supremum value with overline and infimum with underline, the lower and upper box-counting dimensions of a subset F of $\mathbb{R}^n$ can be given by

$$\underline{D_B}F = \underline{\lim}_{\epsilon \to 0} \frac{\log N_\epsilon(F)}{-\log \epsilon}$$

$$\overline{D_B}F = \overline{\lim}_{\epsilon \to 0} \frac{\log N_\epsilon(F)}{-\log \epsilon} ,$$

and the box counting dimension of F by

$$D_B F = \lim_{\epsilon \to 0} \frac{\log N_\epsilon(F)}{-\log \epsilon}$$

---

[2] In practical cases, we will rather be finding ways to identify an average value within the bounds, than determining the bounds, see e.g. [4].

(if this limit exists), where $N_\epsilon(F)$ is any of the following:

1. the smallest number of closed balls of radius ϵ that cover F;

2. the smallest number of cubes of side ϵ that cover F;

3. the number of ϵ-mesh cubes that intersect F;

4. the smallest number of sets of diameter at most ϵ that cover F;

5. the largest number of disjoint balls of radius ϵ with centres in F.

This list is not exhaustive but covers the most frequently found applications of box counting.

3.2. Extending the dimensional formalism to multiplicative fractal measures

A variety of other definitions of dimensions can be introduced, still, in general, they all boil down to the concept of counting the ϵ-covering of the fractal set. In such a case it makes no difference whether the items (of the fractal set) contained in the particular ϵ-coverings belong to one class or differ drastically in some properties. One could give the example of the distribution of bank notes or coins within a certain region or country. Just counting the single occurrences *yes* or *no* of these items in an ϵ-covering does not seems adequate even to a layman. Indeed, tracing the value contained in a certain ϵ-covering would ring a bell with many.

Back to our original purpose of characterising fractals, a multiplicative measure like that on the Cantor set, scales differently from point to point. Recall, for the example of the Besicovitch measure, that for each point of the attractor an 'address' is known which corresponds with the unique sequence of transformations S_i, thus with the product of ratios p_i/s_i, see (6) representing the density increase at each step of refinement. The product being a permutation (Abelian) group, the effective density is not unique for each point - there will be sets of points for which the scaling of density is the same. It is, therefore, straightforward to characterise the object through sets of points that follow the same scaling.

The most sound and comprehensive formalism developed for characterisation of multiplicative measures to date is the thermodymamical formalism by Arneodo et al. [6] In the *micro-canonical* formulation [6] which we outline first, the local scaling component is derived per point from scaling of the measure in the ϵ box. The box $B_x(\epsilon)$ is centered at the point x and the exponent $\alpha(x)$ indicates the rate of scaling at this point

$$\mu(B_x(\epsilon)) \sim \epsilon^{\alpha(x)} \tag{8}$$

This exponent is sometimes referred to as *singularity strength* (and is loosely related to the Hölder exponent in the case of functions). Now, the $f(\alpha)$ *singu-*

larity spectrum describes the distribution of the singularities of the measure in the following sense: [3]

$$N_\alpha(\epsilon) \sim \epsilon^{-f(\alpha)} \ . \tag{9}$$

Thus the $f(\alpha)$ describes the (logarithmic) evolution of the histogram of $N_\alpha(\epsilon)$ when $\epsilon \to 0$, and can be identified with the fractal (Hausdorff) dimension $f(\alpha) = D_B(S_\alpha)$ of a set of points supporting scaling equal $S_\alpha = \{x \in$ *support* $\mu, \alpha(x) = \alpha\}$.

Conceptually straightforward, this (micro-canonical) characterisation is highly unstable in practice due to the naive expectation of uniform scaling of the local exponent $\alpha(x_0)$. In fact, scaling of the measure contained in the box $B_x(\epsilon)$ follows the complicated pattern of the corresponding kneading sequence - the difficulty which can only be surpassed using the *canonical formalism*. It employs the transformation of the global quantity - the partition function $\mathcal{Z}$ defined as

$$\mathcal{Z}(q,\epsilon) = \sum_{i=0}^{N(\epsilon)} \mu_i^q(\epsilon) \ \sim \epsilon^{\tau(q)} \ , \tag{10}$$

where $\mu_i(\epsilon)$ is the measure contained in the i-th box of the ϵ-coverage. Scaling of this partition function $\mathcal{Z}(q,\epsilon) \sim \epsilon^{\tau(q)}$ gives the *mass exponents*

$$\tau(q) = \lim_{\epsilon \to 0} \frac{\log \mathcal{Z}(q,\epsilon)}{\log \epsilon} \ , \tag{11}$$

which can be related to the *spectrum of singularities* through the so-called Legendre transformation (see e.g. [11]):

$$\frac{d\tau(q)}{dq} = <\alpha> (q) \ , \tag{12}$$

$$(f(q))(\alpha) = q <\alpha> (q) - \tau(q) \ . \tag{13}$$

The derivation of the above relations proceeds as follows; let us introduce the Boltzmann weights arising from the partition function $\mathcal{Z}(q,\epsilon)$, (10) as:

$$\mu_i(q,\epsilon) = \frac{\mu_i^q(\epsilon)}{\sum_j \mu_j^q(\epsilon)} \ . \tag{14}$$

The expectation for α, see Eq.(8), over the canonical ensemble is then:

$$<\alpha> (q) = \sum_i \alpha_i \mu_i(q,\epsilon) = \sum_i \frac{\log \mu_i(\epsilon)}{\log \epsilon} \mu_i(q,\epsilon) \ ,$$

---

[3] Note that we use the same symbol $f()$ for the singularity spectrum as in other context for an arbitrary function. This notation is standard in literature and should always be clear from the context.

which can next be directly related to the scaling exponents $\tau(q)$ of the partition function (11) (in the thermodynamic limit of infinite volume $\epsilon \to \infty$ which we assume below):

$$\frac{d\tau(q)}{dq} = \lim_{\epsilon \to 0} \frac{d(\log(\mathcal{Z}(q,\epsilon))/\log(\epsilon))}{dq} = \frac{1}{\log \epsilon} \frac{1}{\mathcal{Z}} \frac{d}{dq} \mathcal{Z}(q,\epsilon)$$

since, from the definition of the partition function $\mathcal{Z}(q,\epsilon) = \sum_i \mu_i^q$, it equals:

$$\frac{d\tau(q)}{dq} = \frac{1}{\log \epsilon} \frac{1}{\mathcal{Z}} \sum_i \log \mu_i(\epsilon) \mu_i(\epsilon)^q = \frac{1}{\mathcal{Z}} \sum_i \frac{\log \mu_i(\epsilon)}{\log \epsilon} \mu_i(\epsilon)^q = <\alpha>(q) \ .$$

If now $f(q)$ is defined as:

$$f(q) = \sum_i \mu_i(q,\epsilon) \frac{\log \mu_i(q,\epsilon)}{\log \epsilon} \ , \tag{15}$$

using (14), one obtains

$$f(q) = q \sum_i \frac{\log \mu_i(\epsilon)}{\log \epsilon} \mu_i(q,\epsilon) - \sum_i \mu_i(q,\epsilon) \frac{\log \mathcal{Z}}{\log \epsilon}$$

which, from (8) and (11) together with the normalisation requirement on the measure μ gives

$$(f(q))(\alpha) = q <\alpha>(q) - \tau(q) \ . \tag{16}$$

The parameter q works as the mechanism to select the singularities of certain strength. For $q > 0$, the partition function is dominated by singularities scaling with $\alpha > 1$. Choosing $q < 0$ increases the role of the singularities of $\alpha < 1$.

Note that for $q = 0$ we recover the original box counting dimension of the set support of the measure. Moreover, it is easy to show that for homogeneous fractals, e.g. self-similar sets with uniformly distributed measure, the $\tau(q)$ is a linear function. The Legendre transformation brings the spectrum of singularities of such measure to one point – exactly the Hausdorff dimension of the support of the measure. It is the non-linearity of $\tau(q)$ which for the generic case contains non-redundant information about the measure distribution and its spectrum of singularities. In the figure below we can see the example $\tau(q)$ and the related $f(\alpha)$ spectrum of singularities for the Besicovitch measure with repartition ratio $p = .3, q = .7$, on the triadic Cantor set support.

4. Beyond the dimensional formalism of fractals

The multi-fractal analysis of multiplicative measures is a definitive step forward in describing fractals arising in many dynamical phenomena in nature. This is, however, still a global characterisation through the fractal dimension of subsets of the measure's support. The information it carries has only statistical meaning and gives only a global sense of the measure's scaling properties. Even
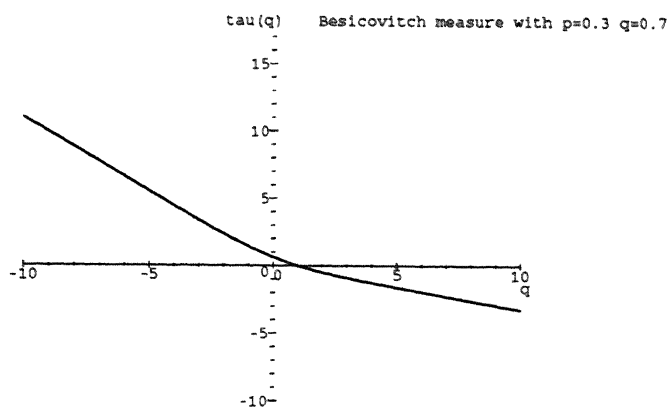
128

tau(q)   Besicovitch measure with p=0.3 q=0.7

FIGURE 11. $\tau(q)$ for the Besicovitch measure $p = .3, q = .7$.

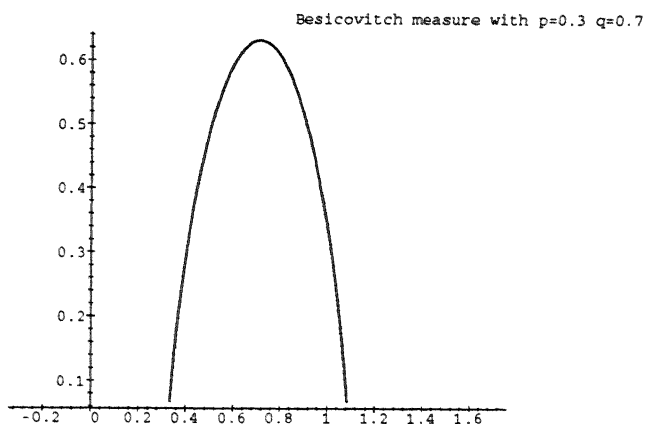Besicovitch measure with p=0.3 q=0.7

FIGURE 12. $f(\alpha)$ for the Besicovitch measure $p = .3, q = .7$.

though it generalises the approach to non-homogeneous measures, it is still unsuitable (in its traditional box counting formulation) for analysing arbitrary fractal *functions* [6].

There is, however, a way of characterising fractals through their primary property, their intrinsic renormalisation, which is reflected in self-similarity or self-affinity. The basic transformations of renormalisation characterising the fractal object are those which are used to create it. In this sense, we can speak of the 'construction rule' associated with the fractal object. Obviously, recovery of such a unique construction rule would provide the most complete characterisation of the fractal. What is perhaps even more striking is the

fact that the 'rule' (subject to an iterative process) could give insight into the dynamics of the process of creation of the fractal object! This is a rather far going expectation, but the primary results obtained are rather promising.

The problem of recovering the invariant renormalisation transformations is generally known as the inverse fractal problem. It was first defined in the context of image compression by BARNSLEY [2], and in its original formulation was only intended to provide a rough approximation tool with a controllable error. This could be achieved through the so-called *collage theorem* [2]. Various approaches were developed, mostly oriented at the decomposition of the *entire* rectangular image through Manhattan (or affine) sub-divisions, while other methods often claiming to solve the Inverse Fractal Problem (IFP) uniquely, aim at finding optimal transformations for *isolated* objects. In both classes of methods there is no intention for the transformations to bear any physical meaning whatsoever. Nor do, to the best of our knowledge, any of the approaches use methods allowing unrestricted recovery of transformations. The restrictions include ad hoc limits on the number of transformations, but also extend over some intrinsic limitations which are inherent to fractal functions, like the inability to single out the scaling behaviour masked by polynomial behaviour.

In our opinion, the problems traditionally encountered in the IFP can successfully be dealt with within the wavelet transformation based approach. Not only does it provide the means to generalise over arbitrary fractal functions and arbitrary type of singularities as recently demonstrated in [7] in the context of multi-fractal formalism but, it also constitutes a representation particularly convenient for localised assessment of renormalisation properties of fractals.

4.1. Wavelet transform in singularity analysis

Of many transforms which can be used to decompose a function, there is one particularly suited to provide localised position-frequency decomposition.

It is the recently introduced wavelet transform, see e.g. [12], which differs from other localised transforms like the Gabor transform in the ability to *zoom in* on very short-lived high frequency phenomena, be it transients in signals or singularities in (fractal) functions.

This ability is achieved in a very simple way through introducing the scale parameter s which 'adapts' the width of the wavelet kernel to the *microscopic resolution* required, thus changing its frequency contents. This action can be performed locally on the investigated function and the location of the *analysing wavelet* is determined by the other parameter b

$$U(s,b)\psi(x) = \psi(\frac{x-b}{s}) \,, \tag{17}$$

where $s, b \in \mathbb{R}$ and $s > 0$ for the continuous version (CWT).

The transform is defined as the inner product of the function $f(x)$ and the thus dilated and translated wavelet $U(s,b)\psi(x)$:

$$(Wf)(s,b) = \frac{1}{s} \int dx\, f(x)\, U(s,b)\, \psi(x) \,. \tag{18}$$

The power given to the normalising factor s, it is often chosen to serve a particular purpose. In this work, in the one dimensional case we choose a default factor s^{-1}, which conserves the integral $\int dx\, |\psi(x)|$ and thus leaves the L^1 measure invariant. [4] This also seems to be the choice generally favoured in most applications of wavelets in fractals to date.

The natural requirement for the wavelet transform would be that of reversibility, that is to say the original function f could be reconstructed from its wavelet transform Wf. This is indeed satisfied as a consequence of the fact that the wavelet transform is an isometric transformation, which can be expressed in the so-called *resolution of identity* for the inner product of the function f and g and their wavelet transforms Wf and Wg: [5]

$$\int_{-\infty}^{\infty} \int_{-\infty}^{\infty} \frac{ds\, db}{s} (Wf)(s,b)(Wg)(s,b) = C_\psi < f,g > \,. \tag{19}$$

The analysis of the local singular properties of a function with the wavelet transform can be illustrated by the following. The singularity strength is often characterised by the so-called Lipschitz-Hölder exponent. If there exists a polynomial $P_n(x)$ of the degree n such that

$$|f(x) - P_n(x - x_0)| \leq C|x - x_0|^h \,,$$

the function $f(x)$ is said be Lipschitz h in x_0, or to have the Hölder exponent h in the point x_0, for $n < h \leq n + 1$. Suppose, the polynomial P_n corresponds to the Taylor series expansion of f around x_0 up to the order n.

It follows directly that if f is equal to a positive integer $n + 1$ it is n times continuosly differentiable in x_0. Alternatively, if $n < h < n + 1$ the function f is continuous and singular in x_0. In that case f is n times differentiable, but its nth derivative is singular in x_0 and the exponent h characterises this singularity. The exponent h, therefore, gives the indication of how regular the function f is in x_0, that is the higher the h, the more regular the function f.

The wavelet transform of the function f in $x = x_0$ with the wavelet of at least n vanishing moments, i.e. orthogonal to polynomials up to (maximum possible) degree n:

$$\int_{-\infty}^{+\infty} x^n \, \psi(x) \, dx = 0 \quad \forall n, \; 0 \leq n < m \,,$$

---

[4] Of course, in the particular case of fractional support of the measure, the invariant measure should be rescaled as s^{-D}, where D is the fractal dimension of the support. However, since this is usually a priori unknown, we will use the default value equal to the embedding dimension of the support, allowing for later possible readjustment.

[5] It can be shown that (19) leads to the so-called *admissibility condition* on the wavelet $\int_{-\infty}^{\infty} dx\, \psi(x) = 0$, which excludes low-pass filters (e.g. the Gaussian). However, since we are only focusing on the renormalisation properties of the object's CWT, we will disregard this restriction.

reduces to

$$W^{(n)}f(s,x_0) \sim C \int \psi(x)|s\,x|^{h(x_0)}\,dx \sim C\,|s|^{h(x_0)} \int \psi(x')|x'|^{h(x_0)}\,dx' \; .$$

Therefore, we have the following proportionality of the wavelet transform of the singularity $n \leq h \leq n+1$, with the wavelet with n vanishing moments, adequately refered to as an *oscillatory box*:

$$W^{(n)}f(s,x_0) \sim |s|^{h(x_0)} \; .$$

The consequences of the ability of accessing the singular scaling behaviour with the wavelet transform and in particular with the modulus maxima representation [13] of the CWT are in fact two-fold. One is the possibility of extending (and correcting) the traditional statistical formalism of fractals [6]. The second, which we would like to pursue further here, is the possibility of recovering the actual renormalisation (scaling) parameters involved in the creation of the fractal attractor through the original *construction rule*.

4.2. Renormalisation recovery from the CWT

Let us first investigate the action of the two element group of our most simple fractal example - the uniform measure on a triadic Cantor set.

$$s^\wedge(1-log(2)/log(3))W(Cantor\_gen6)$$
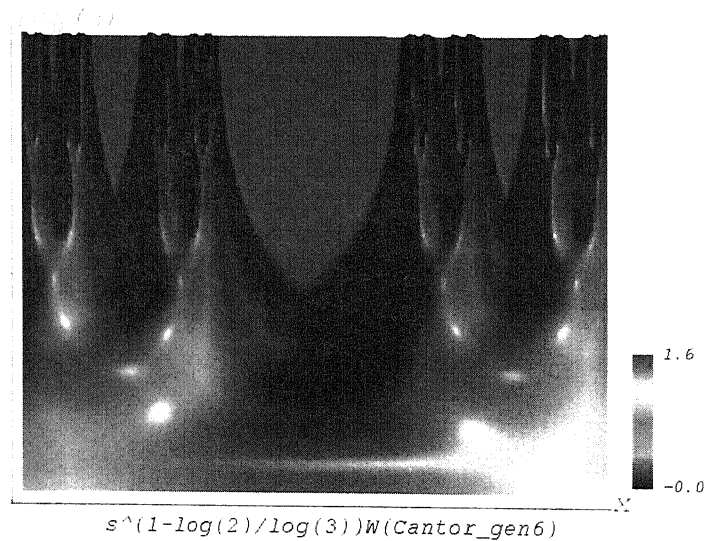
FIGURE 13. The top view on the wavelet transform of the uniform measure on a triadic Cantor set. Note the correction factor equal s^{1-D}, where $D = \log(2)/\log(3)$ is the fractal dimension of the uniform measure on a triadic Cantor set.

132

For the uniform measure on a triadic Cantor set we have the transformation $T_1(1/3, 0)$ and $T_2(1/3, 2/3\,l)$, where l is the length of the initiator $L \equiv F_0$, and $T(a, b)(x) = ax + b = U^{-1}(a, b)$. The function reflecting homogeneous measure distribution on a triadic Cantor set f_C is thus invariant with respect to these two transformations, see theorem 1 in chapter 2:

$$f_C = \bigcup_{1,2} T_{1,2} f_C \tag{20}$$

The wavelet transform of the uniform measure on a triadic Cantor set f_C is thus for T_2:

$$
\begin{aligned}
(Wf)(s, b) &= \int s^{-1} dx \; f(x) \; U(s, b) \; \psi(x) \\
&= \int s^{-1} dx \; T_2(1/3, 2/3\,l) f(x) \; U(s, b) \; \psi(x) \\
&= \int s^{-1} dx \; f(1/3\,x + 2/3\,l) \; \psi(\frac{x - b}{s}) \; .
\end{aligned}
$$

On taking $x' = 1/3\,x + 2/3\,l$ we obtain

$$
\begin{aligned}
(Wf)(s, b) &= \int s^{-1} 1/3^{-1} dx' \; f(x') \; \psi(\frac{x - b}{s}) \\
&= \int s^{-1} 1/3^{-1} dx' \; f(x') \; \psi(\frac{x' - 2/3\,l - 1/3\,b}{1/3\,s}) \\
&= (Wf)(1/3\,s, 2/3\,l + 1/3\,b) \; .
\end{aligned}
$$

We see that the invariance in the fractal attractor reflects in the invariance of the wavelet transform with respect to the operator T_2. Analogically, for the operator T_1 we obtain $(Wf)(s, b) = (Wf)(1/3\,s, 1/3\,b)$. While this fact can be verified in the figure showing CWT of the investigated attractor, it is much more convenient to observe it in the so-called *wavelet transform modulus maxima* (WTMM) representation – as pointed out by MALLAT [13], a representation reduced to the local (modulus) maxima in x of the wavelet transformation $(Wf)(s, x)$ of a function $f(x)$ can be considered to be complete for a large class of functions.

In the figure showing the WTMM of uniform measure on a triadic Cantor set, Figure 14, the invariance with respect to the operators T_1 and T_2 is immediately apparent and is emphasised with the help of windows.

While perhaps not most spectacular for the uniform measure on the Cantor set exactly the same reasoning can also be applied to more complicated measures and in general to arbitrary functions. Let us now take the example of the Besicovitch measure. The continuous wavelet transform (CWT) of the example mass repartitioning using 0.3/0.7 ratio, on the support of the uniform triadic Cantor set, is shown in Figure 15 below.
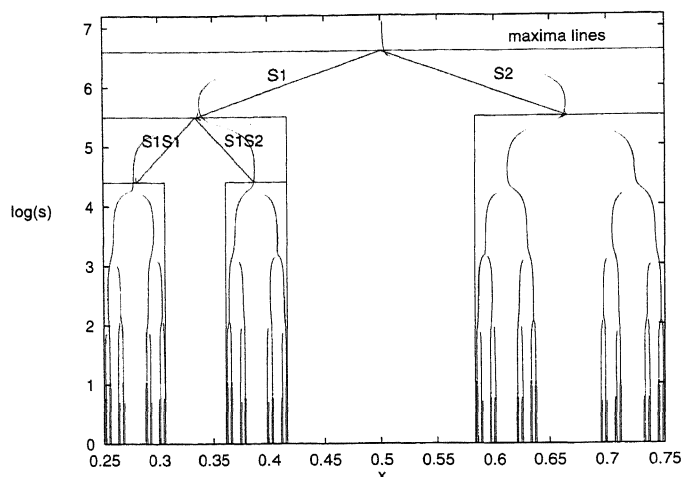
FIGURE 14. The top view of the maxima representation of the wavelet transform of the uniform measure on a triadic Cantor set. The two renormalisation transformations are shown and the corresponding renormalised windows can be compared by overlaying.

Recall that (6) describes the transformation used to create this invariant self-affine object. At the same time, they constitute the invariance transformations corresponding with the object. If we now identify two operators acting on scale and position as $T(c_1^{-1}, b_1/c_1)$ and $T((c_2^{-1}, b_2/c_2))$, we directly have

$$(Wf)(s,x) = (W)[p_{1,2}T_{1,2}(u,v) \, f](s,x) = p_{1,2}(Wf)(s',x') \,, \qquad (21)$$

for the scale-position coordinates of the related bifurcations:

$$(s,x) = [T_{1,2}(u,v)](s',x') = (u_{1,2}s' \,, \, u_{1,2} \, x' + v_{1,2}) \qquad (22)$$

Thus the pair of vectors $(\overline{ss'}, \overline{xx'})$ constitutes the two components (position, scale) of the invariance vector in the scale-position domain. An illustration of this is given in Figure 16. The top window and its two images renormalised back for comparison are shown overlayed on top of one another. The task of tracing the invariance in question is now easier since the scaling component $\overline{ss'}$ becomes a vector in the scale-position plane just like the translation component $\overline{xx'}$. If we follow the resultant vector (after renormalisation, up to finite size distortions) we find the same pattern again.

However, the invariance in the scale position plane only defines the two components of the invariance vector. The renormalisation transformations for the investigated measure take their complete form only if we include the information (regarding the repartitioning of measure) contained in the values of the wavelet transform in the corresponding renormalising bifurcations, as evident from (21):

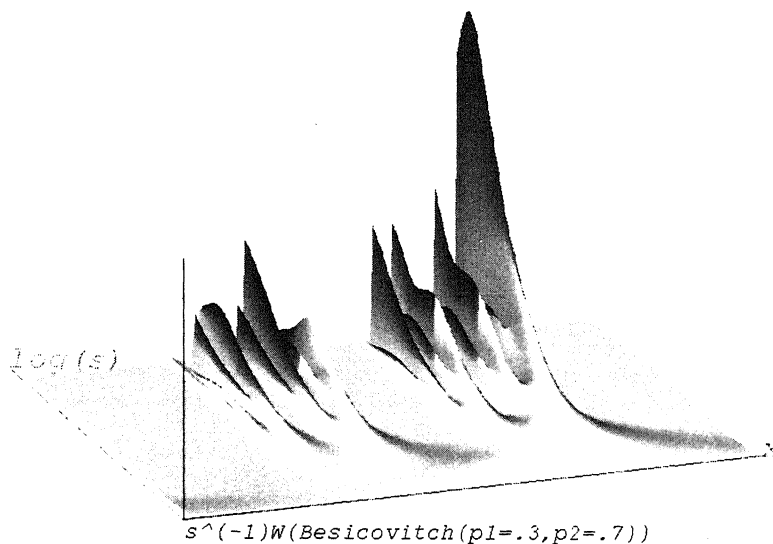$$s^{\wedge}(-1)W(Besicovitch(p1=.3,p2=.7))$$

FIGURE 15. The wavelet representation of the Besicovitch measure with mass repartition 0.3/0.7, on the support of the uniform triadic Cantor set. The wavelet used is the Gaussian.

$$\frac{(Wf)(s,x)}{(Wf)(s'_{1,2},x'_{1,2})} = p_{1,2} \, . \tag{23}$$

It is, therefore, possible to reveal all the original renormalisation parameters (constituting the originally addressed 'construction rule') from the wavelet transform bifurcation representation of the investigated fractal.

Recovering the invariance in question and determining the degree of its uniformity is the main challenge in solving the Inverse Fractal Problem. The actual key to the solution of the inverse fractal problem using the CWT is utilising the invariant 'landmarks' in the wavelet landscape – the bifurcations [3, 8]. The coordinates of these objects are subject to the transformations to be identified; therefore, finding sets of bifurcations following the same transformation gives access to the transformation itself. Let us therefore state the following: *If an object is invariant with respect to some construction rule S, it is self-affine (self-similar) and is a fractal.* **The Inverse Fractal Problem** aims at recovering the unknown construction rule in order to prove that the object F is self-affine (self-similar).

This is in general a rather difficult task, but we will demonstrate that it is a feasible one – the possibility to do this is contained in the invariant representation such as the bifurcation representation. The rationale behind focusing on the bifurcation points is similar to that for the modulus maxima - the particularly convenient feature of this representation is its translation invariance,
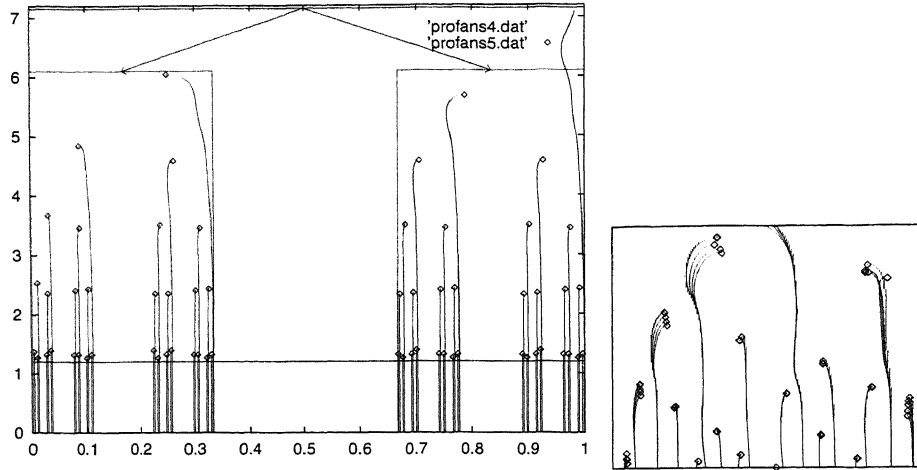
135

FIGURE 16. The wavelet bifurcation and maxima representation of the Besicovitch measure with mass repartition 0.3/0.7, on support of the uniform triadic Cantor set.

which is of great importance in pattern recognition problems. Since fractal functions are a special class of functions where the translation invariance is accompanied by scale invariance, representation invariant with respect to both scale and position shift is required. In searching for a representation featuring such unique 'landmarks', we found very suitable the bifurcations of the maxima lines, defined to be the points in the scale-space domain where a new maxima line begins while going towards smaller scales. These points can be identified as *general maxima* of the wavelet transform i.e. as points where $|Wf(s,x)|$ is locally maximum in a two dimensional neighbourhood of (s_0, x_0) in the scale-position plane.

The necessary condition for the general maximum is the zero of the derivatives along both the position x and the scale s directions.

$$\begin{cases} \frac{d(Wf)(s,x)}{dx} = 0 \\ \frac{d(Wf)(s,x)}{ds} = 0. \end{cases} \tag{24}$$

In Figure 17, we indicate the action of the transformation S_1 on two bifurcations B_1 and B_2. Although arbitrary in principle, we prefer to choose bifurcations most upward in scale/hierarchy; the explanation of the reasons for this will be given in the next chapter. The action of both the transformations results in the bifurcations $B_1' = S_1(B_1)$ and $B_2' = S_1(B_2)$ respectively. Next, B_1'' and B_2'' are indicated as the results of respectively, $S_1(B_1')$ and $S_1(B_2')$, and so on.... In the right figure we find a similar analysis in the case of S_2.

This means, that for each pair of bifurcations there is a sequence of transformations S_i relating them, and vice versa, there are subsets of bifurcations,
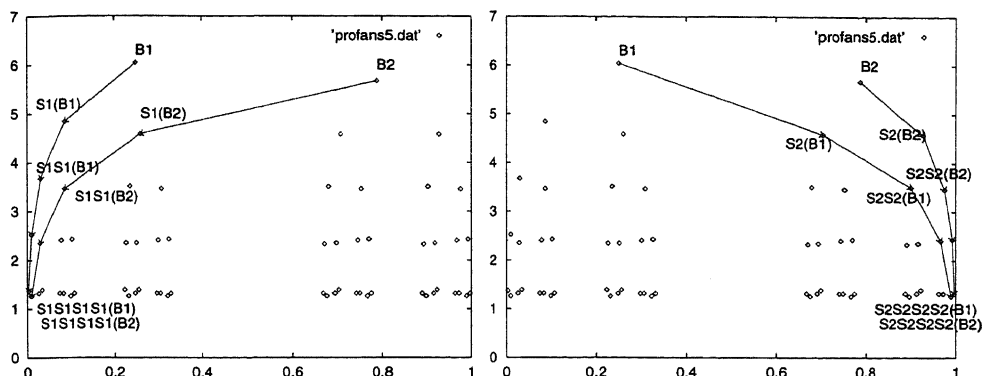
FIGURE 17. The action of the transformation S_1 on two arbitrary bifurcations B_1 and B_2 results in the bifurcations $B'_1 = S_1(B_1)$ and $B'_2 = S_1(B_2)$ respectively. Next, B''_1 and B''_2 are indicated as the results of respectively, $S_1(B'_1)$ and $S_1(B'_2)$, and so on.... In the right figure, similar analysis for the case of S_2.

for which the transformation is either S_1 or S_2 - a few of which are shown in the figure above 17.

If we were to check for all the possible pairs of bifurcations to which transformation their coordinates are subjected, we would discover that the most common transformations are in fact the pair S_1 and S_2. Of course, there would be many combinations of the transformations occurring quite often, but always less frequently than the two primary ones. Moreover, once all the pairs of bifurcations subject to the 'strongest' pair of transformations are removed from the representation, there would be almost no bifurcations left (except for those not matched due to errors).

This is a very intuitive description of the procedure we have developed to identify invariance in the bifurcation representation and it indicates the following facts: [6]

1. We seek for the most *consistent* transformations, that is such which transform the largest sets of bifurcations; later we will introduce measures for estimating this purpose;

2. since any combination of the invariance transformations is again an invariance transformation, our purpose is finding the *irreducible* elements of the group of transformations, therefore each pair of successfully matched bifurcations can in principle define only one invariance transformation.

---

[6] For the more complete description of the numerical algorithm, we refer the reader to the next subsection, as well as to [8, 4].

137

The sets of bifurcations thus isolated, related through either of the transformation S_1 and S_2, can be now used to reflect the original global invariance transformation in (probabilistic) distributions of parameters of the invariance model Figure 18. The modes of these parameter distributions evaluated for the investigated example show remarkable agreement with the original values.

The information contained in the modes of the parameter distributions is complemented by the particularly interesting information obtained by relating the coordinates of the matched bifurcations. The coordinates transform according to $T_{1,2}$ as indicated in (22), therefore if we set off the position coordinate of the bifurcation upper in scale with the matching bifurcation lower in scale for all matched bifurcations, see Figure 18, we obtain the *dynamic* maps directly! The maps encompass the generation rule which governs the creation of the object in a dynamical process $x(t) \rightarrow x'(t + \Delta t)$, where t denotes time evolution.
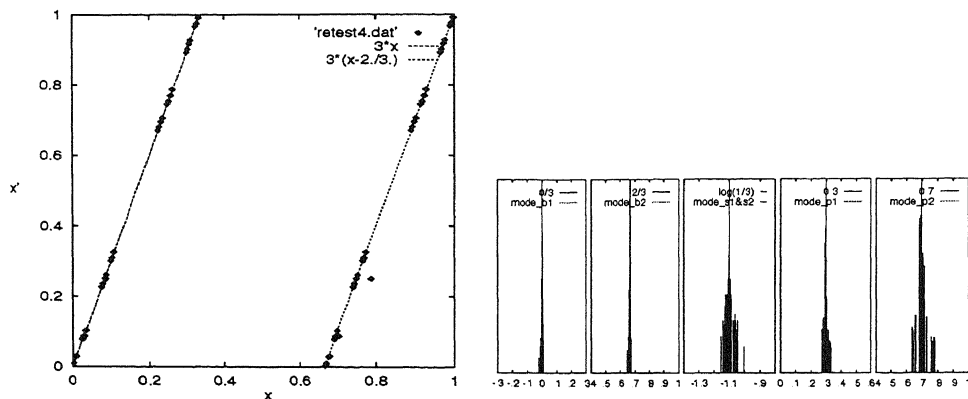
FIGURE 18. The x coordinates of matched bifurcations transformed according to the linear mappings T_1 and T_2 (left). The modes of the parameters of the invariance transformations S_1 and S_2. From left to right $b_1 \approx 0/3$, $b_2 \approx 2/3$, $s_{1,2} \approx \log(1/3)$, $p_1 \approx 0.3$, $p_2 \approx 0.7$. (right)

Note, that the distribution of the points on the maps reflects the structure of the support of the attractor – the uniform triadic Cantor set!

Let us now move to the general self-affine function as shown in Figure 7. Such a function cannot be expressed as a simple multiplicative map, due to the fact that it contains a (piecewise linear) polynomial which constitutes the 'background' of the multiplicatively scaling function. In general, the background polynomials may or may not themselves be introduced by the iterative affine mapping. As such, they may well consist of relevant information, but also may well simply be completely irrelevant to renormalisation properties, and therefore can often rightly be referred to as noise. However, they will always be masking the multiplicative renormalising of the object, and removing

arbitrary noise of this kind is often crucial for the recovery of the renormalisation properties of the object.

The self-affine function can generally be described by a set of a finite number n of self-affine transformations of the generic form

$$f_n{}'(x) = S_n(f_n(x)) = \alpha_n \, f_n((x - \beta_n)/\sigma_n) + \gamma_n \, (x - \beta_n) + \delta_n, \; n \in N \,. \tag{25}$$

Therefore taking the wavelet with two vanishing moments we will be able to capture the invariance of the operators acting on scale and position:

$$(D^{(2)} f')(x) = \alpha_n \, (D^{(2)} f)(\frac{x - \beta_n}{\sigma_n}) \sigma_n{}^{-2} \tag{26}$$
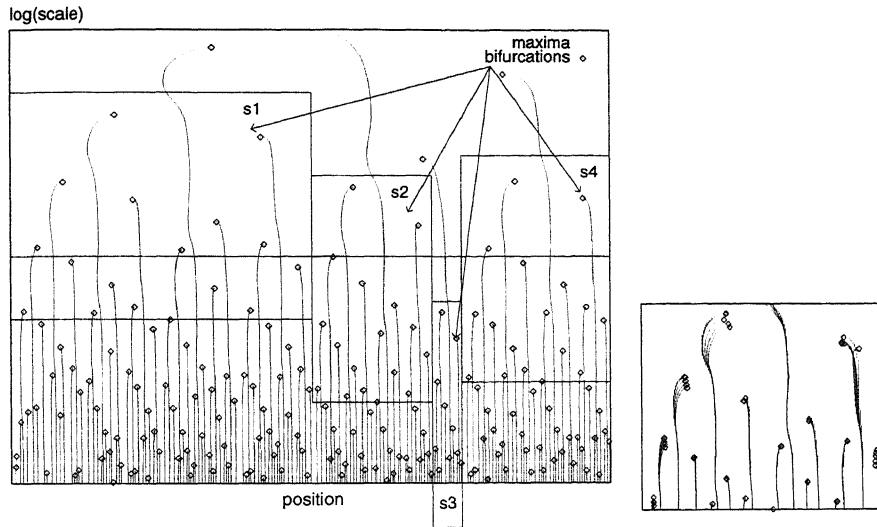
FIGURE 19. Windows on the wavelet maxima representation of the self-affine function (left). Comparison of the windows by means of renormalising and overlaying (right).

See Figure 19 for the indication of the invariance present in the example discussed. The remaining information can be assessed by decomposing the self-affine function into the wavelets with an increasing number of vanishing moments $\psi^{(0)}$, $\psi^{(1)}$, $\psi^{(2)}$. It allows us to solve the set of equations:

$$\begin{cases} f'(x) &= \alpha_n \, f(\frac{x-\beta_n}{\sigma_n}) + \gamma_n \, (x - \beta_n) + \delta_n \\ (D^{(1)} f')(x) &= \alpha_n \, (D^{(1)} f)(\frac{x-\beta_n}{\sigma_n}) \sigma_n{}^{-1} + \gamma_n \\ (D^{(2)} f')(x) &= \alpha_n \, (D^{(2)} f)(\frac{x-\beta_n}{\sigma_n}) \sigma_n{}^{-2} \end{cases} \tag{27}$$

by means of comparing corresponding f and f' values (and their D and $D^{(2)}$ derivatives) on the invariant structure of bifurcations recovered from wavelet transform performing the second derivative of the investigated function $W^{(2)} f$:
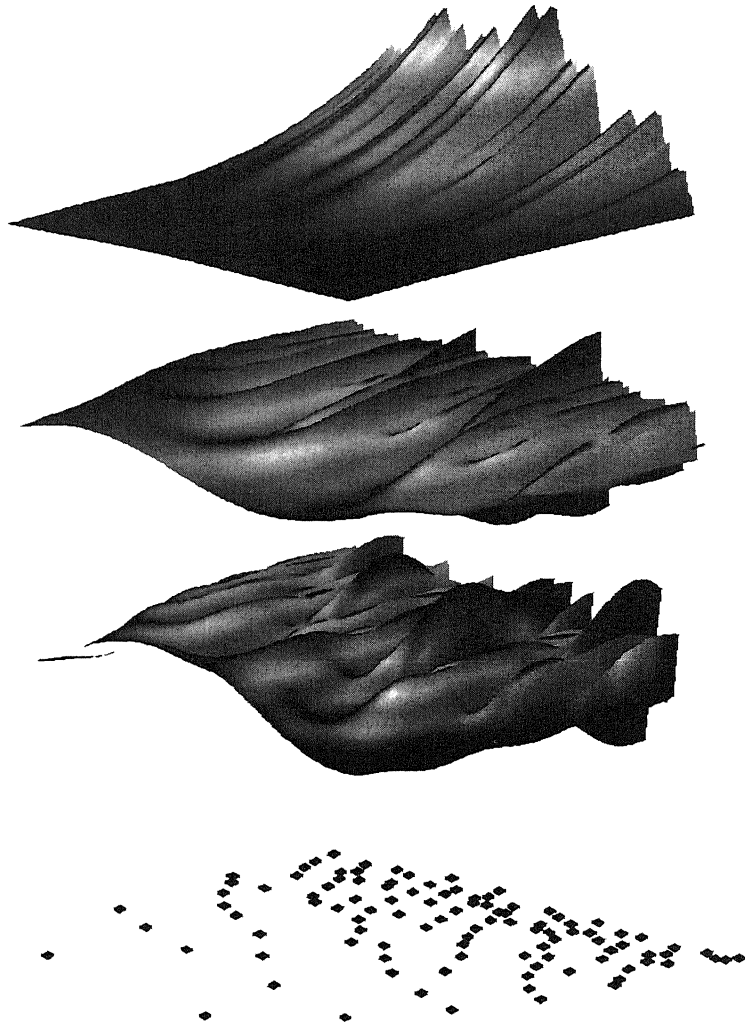
139

FIGURE 20. A stack of wavelet transforms $W^{(2)}f$, $W^{(1)}f$ and $W^{(0)}f$, sampled with the affine grid of bifurcations.

$$\begin{cases} x' &= \sigma_n x + \beta_n \\ s' &= \sigma_n s \end{cases} \text{ and } (W^{(2)}f_n{}')(s',x') = \frac{\alpha_n}{\sigma_n{}^2}(W^{(2)}f_n)(s,x) , \quad n \in \mathbb{N} . (28)$$

Using estimated parameters $\sigma_n, \beta_n, \alpha_n$, we can, in sequel, solve the set of equations (27) by sampling the corresponding wavelet decompositions on the recovered invariant grid; see Figure 20 for an intuitive illustration of this idea.

For all the parameters, expectations were obtained by estimating the mode of parameter distribution and have shown good agreement with the values
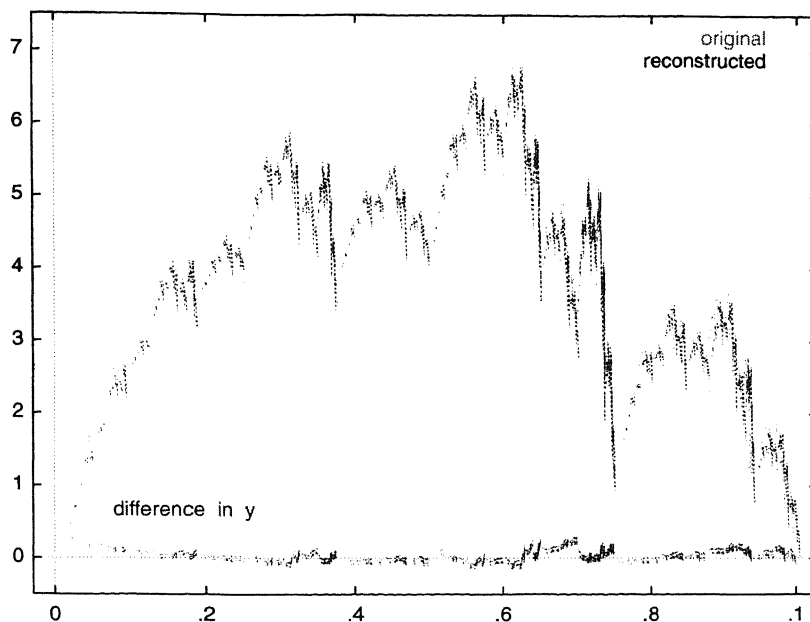
FIGURE 21. The original attractor, the attractor reconstructed using the set of revealed self-affine transformations and the difference in y between the two attractors. (The error on the orthogonal x coordinate not shown in the figure is of the same order.)

used to construct the self-affine example. We refrained from displaying all the individual (twenty) modes. Instead, we show the result of the reconstruction of the self-affine attractor with the estimated maps, Figure 21.

4.3. A General tree mapping algorithm

The essence of this method lies in finding best matches in the hierarchy of bifurcations derived from the structure of the wavelet maxima representation. In order to construct such a hierarchy, each maximum line of the wavelet maxima representation will be associated with a *branch*. We say that the bifurcation $b(s, x)$ *belongs* to the branch h_i (or is *visible*) if, at the scale s there is no other branch h_j between h_i and $b(s, x)$:

$$b(s, x) \ belongs\ to\ h_j \quad \Leftrightarrow \quad (line\ segm[b(s, x), h_i] \cap h_j = \emptyset \ , \forall j \neq i) \ . \quad (29)$$

One bifurcation will, therefore, belong to the two closest maxima lines h_p and h_q, on both sides of the bifurcation. (The boundary cases will be treated in a wrap-around fashion.) We will associate probability measures with this relation of bifurcations to branches as follows: the probability that the bifurcation $b(s, x)$ belongs to the branch h_p is:
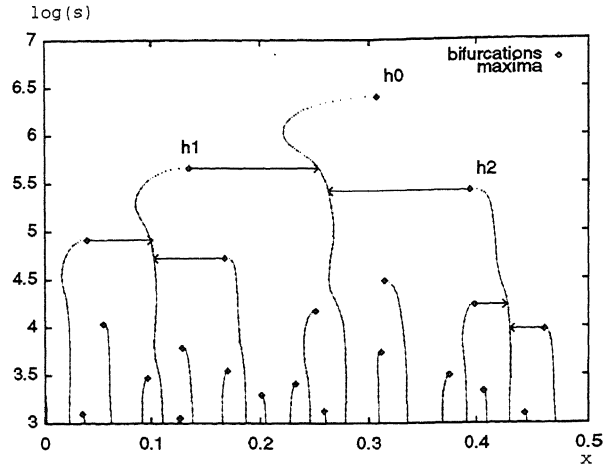
FIGURE 22. Construction of a tree in the left figure, and the same tree now as a sub-tree (one of the main four) within the complete representation on the right. We used the example self-affine function from Figure 21. Maxima lines are left visible in order to facilitate perception of the trees. Only the more probable relationships are shown.

$$P(b(s,x) \ belongs \ to \ h_p) = \frac{distance(b,h_q)}{distance(b,h_p) + distance(b,h_q)} \tag{30}$$

where $distance(a,b) = |x_s(a) - x_s(b)|$ i.e. it equals the Euclidean distance between the x coordinates of the maxima lines at a certain scale s. Obviously, $P(b(s,x) \ belongs \ to \ h_q) = 1 - P(b(s,x) \ belongs \ to \ h_p)$, and by this definition the probability P is drawn from a uniform distribution.

Since a new branch originates from each bifurcation, we will define a *tree* as a couple consisting of a branch h and all trees originating from the bifurcations b_l belonging to the branch h

$$tree(h) = (h, \{tree(h_l)\}) : (h_l \cap b_l \neq \emptyset \land (b_l \ belongs \ to \ h))) \ . \tag{31}$$

In Figure 22, we illustrate the first few steps of the process of tree creation. It is apparent that since a new tree is defined for each maximum line, one bifurcation can belong to many trees.

This completes the creation of the probability relationships in the bifurcation representation. For N_{tot} bifurcations, we have $2^{N_{tot}-1}$ arrangements which form a valid tree. The task of the algorithm is to explore the search space in order to find the most likely arrangement, while avoiding a combinatorial explosion of the computation.

The topology of the arrangement found determines which sub-trees are present in the tree, therefore determining the maps which characterise the system. Referring to a generic tree, see Figure 23, we will be able to distinguish

142

three main branches
of the generic tree:

two side branches
and shift root

the top root of the hierarchy

pruned from the
three main branches
there are possible
branches lower in
the hierarchy

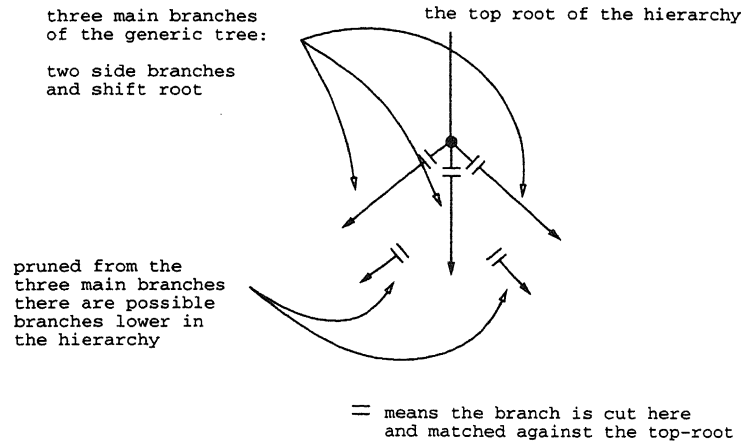$=$ means the branch is cut here
and matched against the top-root

FIGURE 23. The branching of a generic tree. See text for description.

left and right branches and the root. The most obvious first match would be between the first side branch, that is the highest in the hierarchy, and the complete tree. In the same way, the next match would be with the side branch on the opposite side, assuming there is one there. The third step is perhaps less obvious; after pruning the first two side branches we can try matching the remaining *radical shift* sub-tree against the original top-tree. [7] In all these steps, each bifurcation can be used only once, thus its assignment becomes restricted to one sub-tree only, and therefore it takes part in defining only one map.

Naturally, in most cases there will be bifurcations which do not match. The existence of trees stemming from these bifurcations indicates that potentially there are more than three maps in the system. Therefore, any sub-tree pruned in these three generic matches is next used for subsequent matching against the complete top-tree as before. A description of the tree/sub-tree matching algorithm used in the above procedure will follow.

This hierarchical approach constitutes the first heuristic used to limit the search space. The motivation for this is that the higher the sub-tree is in the hierarchy, the more likely it is to acquire a large likelihood measure, due to the larger scale extent it can cover. Therefore, it can potentially contribute largely to the maximisation of the total likelihood measure.

The likelihood measure being maximised is:

$$Measure = \frac{\sum_{m=1}^{M} \left[\left(\frac{n_m}{N_{tot}}\right)^a \left(\prod_{i=1}^{n_m} P_i^{low} P_i^{high}\right)^{1/n_m} f(\tilde{\sigma}_m)\right]}{Norm(a,b)}, \quad (32)$$

[7] In practice it is this radical shift that is tried first, all pruned branches constituting the sub-trees.

where $f(\tilde{\sigma}_m)$ is a penalty factor

$$f(\tilde{\sigma}_m) = e^{-b \sqrt{\sum_k \sigma_k^2}}.$$

The factor n_m/N_{tot} determines the fraction of the bifurcations used while $\prod_{i=1}^{n_m} P_i^{low} P_i^{high}$ is the total likelihood of matched bifurcations. M is the number of maps extracted and $Norm(a, b)$ is intended to normalise the measure with respect to parameters a and b. Since we obtained a reliable performance for constant, minimal assumption based values of $a = 2$ and $b = 1$, the optimisation with respect to these parameters proved unnecessary and the norm $Norm(a, b)$ could also be neglected.

The argument for such a construction of the measure is as follows: the 'average' likelihood is computed over all n_m matched branches (i, j) as $(\prod_{i=1}^{n_m} P_i^{low} P_i^{high})^{1/n_m}$. This measure ingredient alone will, however, tend to favour a minimal number of bifurcations per map n_m. In order to compensate for this, we introduced the $(n_m/N_{tot})^{a/2}$ factor. The measure constructed in this way can already be used quite reliably.

To improve the ability to avoid gross errors in the map construction, we introduced a penalty factor taking into account the standard deviation of the constructed maps with respect to a linear fit to the map. The total normalised standard deviation $\sqrt{\sum_k \sigma_k^2}$ in an exponent over e is used to suppress only large deviations. The factor b in $f(\tilde{\sigma}_m)$ was left at $b = 1$. This ingredient of the total measure also required compensation with the $\left(\frac{n_m}{N_{tot}}\right)^{a/2}$ factor. And similarly as for b, we obtained the best results for the minimal choice of $a = 2$.

In detail, the tree/sub-tree matching algorithm proceeds as follows: for the two roots, referred to as (l)ower and (h)igher, the bifurcations belonging to these roots, (j, k) respectively, are matched within a predefined depth $(j+/-d, k+/-d)$. This is a very important restriction on the search space, since only the visible bifurcations (those for which the probability (30) can be defined) are taken into consideration. Now we check whether the selected pair (j, k) satisfies a number of criteria, ensuring a certain level of local scaling consistency. In the current version of the algorithm, we choose the following tests for the pairs bifurcations: they must lie on the same side of the root, the probability of the bifurcation at the (l)ower root is higher than the threshold parameter T_{prob}, the correlation of the probabilities exceeds the current value of the threshold parameter T_{corr}, and the correlation of the wavelet transform values of both bifurcations is positive.

If all the tests are passed, the two roots stemming from j and k are processed in the same fashion as the h and l roots above. The process, schematically illustrated in Figure 24, continues recursively in a depth-first fashion. Apparently there is no reason not to use the breath-first search here. In this case all the bifurcations belonging to the considered lower and upper roots would be processed before going down in hierarchy.

The thresholds T_{corr} and T_{prob} are then independently varied and the global maximum of the measure is sought. The maps obtained from the match with
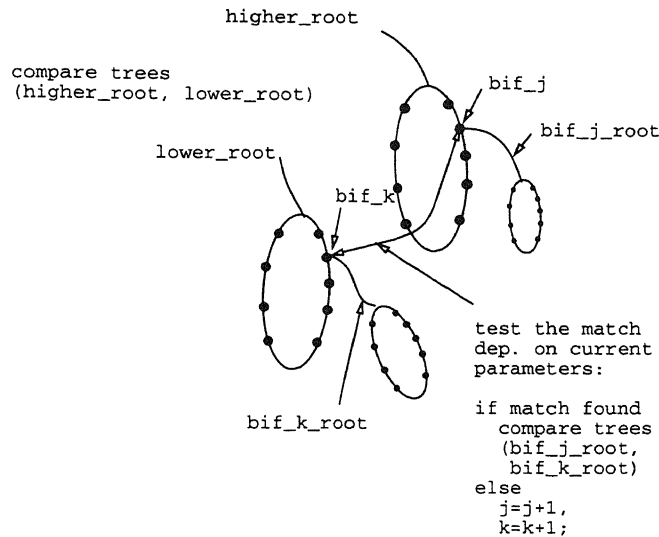
FIGURE 24. The bifurcation matching algorithm. See text for description.

the parameters corresponding with the maximum measure are supposed to be the most probable maps.

A convenient way of visualising the maps (22) is plotting the coordinates x' and x of matched points against one another. In Figure 25, we show automatically recovered maps between x and x' for the self-affine function shown in Figure 7, using the tree matching algorithm. Indeed, the linearity of the maps is evident.

Even though throughout this work we limited ourselves to linear transformations, we would like to point out here that the methodology presented also works in case of small deviations from linearity. The ability to capture non-linear behaviour can be of great value in applying this methodology to physical sciences. As an example test case to test the ability of the algorithm to recover non-linear maps, we generated an attractor with maps modulated with $x \sin(x)$. The example result is shown in Figure 26 together with the plots of the original maps. We considered the agreement of the experiment with the original maps to be quite satisfactory.

5. A NOTE ON TWO-DIMENSIONAL EXTENSION

5.1. Fractal IFS functions in two-dimensions

In this section, we will address only a few relevant facts about self-affine functions over two-dimensional (or fractal $1 < D < 2$) support. We will consider continuous contraction transformations $S_i : \mathbb{R}^3 \to \mathbb{R}^3$, in short to be called maps, chosen in such a way that the self-affine set they define is a functional
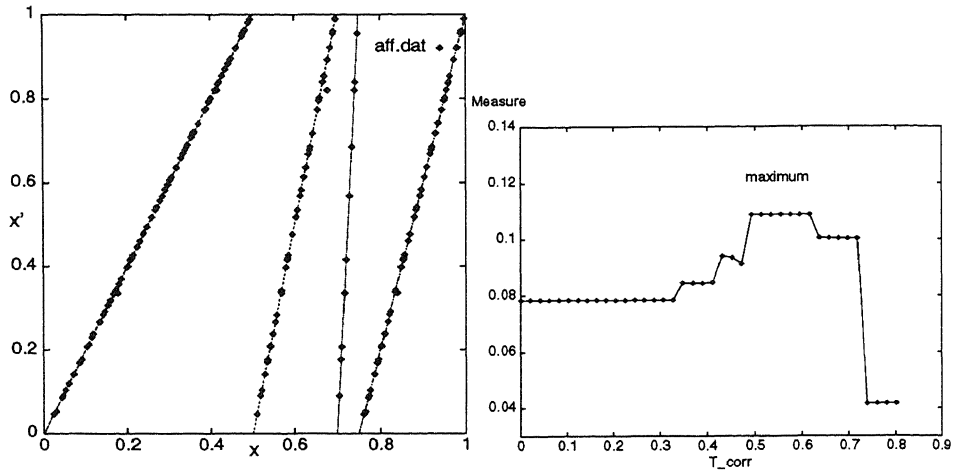
FIGURE 25. In the left figure, maps: $x' = \sigma_n x + \beta_n$ recovered automatically with the tree matching algorithm, and in the right figure, a cross-section through the measure (5.5) with the 'plateau' of maximum value indicated. The section is taken with T_{corr} as free variable. The self-affine function is taken from Figure 21.
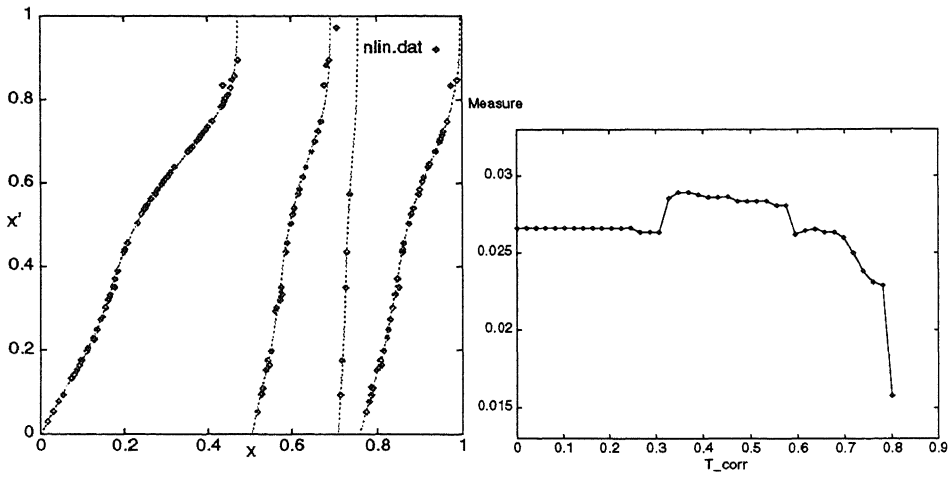

FIGURE 26. In the left figure, maps recovered from the attractor generated with maps modulated with $x \, sin(x)$, in the right figure, a cross-section through the measure (Eq. (5.5)) with T_{corr} as free variable.
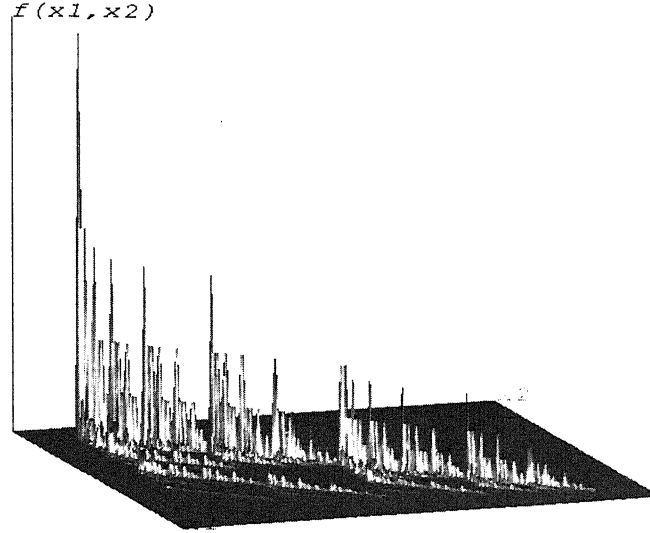
FIGURE 27. The test case: Sierpiński triangle with non-uniformly distributed measure.

mapping $f : \mathbb{R}^2 \to \mathbb{R}$.

Let S_n ($1 \leq n \leq N$) be an affine transformation represented in matrix notation with respect to the coordinates (x_1, x_2, y) by

$$S_n \begin{pmatrix} x_1 \\ x_2 \\ y \end{pmatrix} = \begin{pmatrix} a_n & b_n & 0 \\ c_n & d_n & 0 \\ \gamma_{n1} & \gamma_{n2} & \alpha_n \end{pmatrix} \begin{pmatrix} x_1 \\ x_2 \\ y \end{pmatrix} + \begin{pmatrix} e_n \\ f_n \\ \delta_n \end{pmatrix}. \tag{33}$$

For the sub-transformation on the coordinates $\{x_1, x_2\}$ of the function $F(x_1, x_2)$:

$$S_{xn} \begin{pmatrix} x_1 \\ x_2 \end{pmatrix} = \begin{pmatrix} a_n & b_n \\ c_n & d_n \end{pmatrix} \begin{pmatrix} x_1 \\ x_2 \end{pmatrix} + \begin{pmatrix} e_n \\ f_n \end{pmatrix} \tag{34}$$

which describes an arbitrary affine transformation in $\mathbb{R}^2$, we will require

$$0 < \sigma_n^{-1} = \begin{vmatrix} a_n & b_n \\ c_n & d_n \end{vmatrix} < 1$$

where $|\bar{\bar{S}}| \equiv \det \bar{\bar{S}}$, which ensures that S_{xn} is a similitude and the transformed surface does not vanish or flip over. We will also restrict S_{xn} to be a set of non-overlapping transformations:

$$S_{xi}(A) \cap S_{xj}(A) = \emptyset, \quad \forall i \neq j, \quad \forall A,$$

where A is a compact set.

Additional constraints can be specified for the purpose of generating a fractal interpolation surface ensuring joining up of the transformed surfaces at the interpolated points. [8] For the complete version of the IFS surfaces generation scheme on two dimensional support, the reader may wish to consult Geronimo et al. [14].

The extension of the wavelet transform to two dimensions is straightforward: again the (real-valued) wavelet transform W decomposes the function $f(\mathbf{x}) \in L^2(\mathbb{R}^2)$ in the base of elementary wavelets created by the action of the affine group on a single function $\psi(\mathbf{x})$:

$$(Wf)(\bar{\bar{S}}, \mathbf{b}) = \frac{1}{|\bar{\bar{S}}|} \int d\mathbf{x}\, f(\mathbf{x})\, U(\bar{\bar{S}}, \mathbf{b})\, \psi(\mathbf{x}) \tag{35}$$

where

$$U(\bar{\bar{S}}, \mathbf{b})\psi(\mathbf{x}) = \psi((\bar{\bar{S}})^{-1}(\mathbf{x} - \mathbf{b})).$$

As before, the wavelet $\psi(\mathbf{x})$ is often chosen to be well localised both in scale and space, and if no directional sensitivity is required, uniform scaling in all directions is a natural choice. The matrix $\bar{\bar{S}}$ can then be reduced to two equal scaling factors s on the diagonal and $|\bar{\bar{S}}| = s^2$. This is the choice we will favour here.

The necessary condition for the local extrema of the wavelet transform $Wf(s, x_1, x_2)$ of the function of two variables $f(x_1, x_2)$ is zero of the partial derivatives:

$$\begin{cases} \frac{\delta(Wf)(s,x_1,x_2)}{\delta x_1} &= 0 \\ \frac{\delta(Wf)(s,x_1,x_2)}{\delta x_2} &= 0 \,, \end{cases} \tag{36}$$

which points are further classified according to the sufficient condition for local extrema:

$$\begin{cases} \mathcal{H}(s,x_1,x_2) &> 0 \\ \frac{\delta^2(Wf)(s,x_1,x_2)}{\delta x_1^2} &< 0\, (>0) \end{cases} \tag{37}$$

in the case of a local maximum (minimum), where $\mathcal{H}(\cdot)$ is the Hessian

$$\mathcal{H}(\cdot) = D^{(2)}_{x_1^2}(Wf)(\cdot)\, D^{(2)}_{x_1^2}(Wf)(\cdot) - \left(D^{(2)}_{x_1,x_2}(Wf)(\cdot)\right)^2.$$

The bifurcation case is defined by:

$$\begin{cases} Equation\ (36) \\ \mathcal{H}(s,x_1,x_2) &= 0\,. \end{cases} \tag{38}$$

---

[8] These conditions are, however, irrelevant for this work. In fact, for the sake of simplicity, we will limit ourselves to examples without additional components in the function value which translates to $\gamma_n = 0$ and $\alpha_n = 0$.
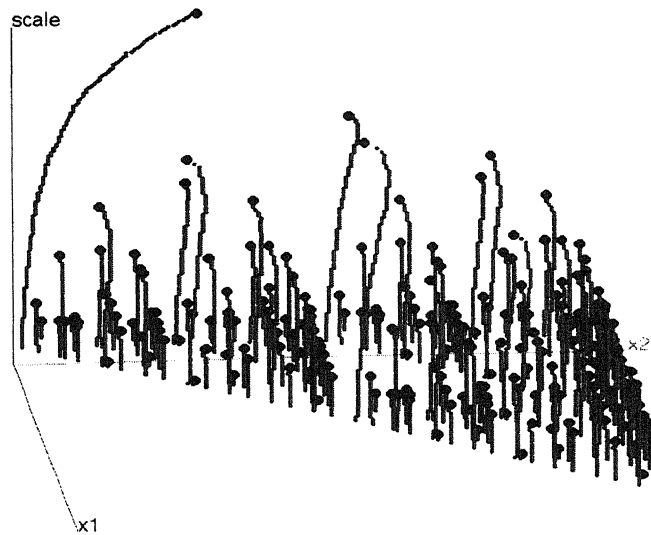
URE 28. Local maxima of the wavelet transform with associated bifurca-
ιs for the example from figure 1. The wavelet used is the Gaussian, $m = 0$.

The tree structure apparent in the maxima representation serves as basis
the parameter recovery algorithm utilised in the solution to the IFP. The
ι construction is similar to that described for the one-dimensional case. The
t crucial step comprises the finding of the invariance of the bifurcation rep-
ιntation. This can be done by means of tree matching, where the invariance
he representation is sought in the optimal match of the tree to its branches.
m the match of pairs of bifurcations found invariant, the parameters of (33)
estimated.

For an elaboration on the differences with the one-dimensional case, we
ιr the reader to [4]; here we will restrict ourselves to presenting and inter-
ting the results for the given example. The affine maps $x_{\{1,2\}} = f(x_1', x_2')$
resenting scaling and translation parameters of S_{x_n} as shown in Figure 29.
expected from the diagonal character of S_{x_n} for the Sierpiński triangle the
ιar dependence with consistent slope $1/\sigma_n = 1/0.5$ shows in only one of the
ιrdinates.

A WORD OF CONCLUSION

e aim of this communication is to share our opinion that the application
the CWT based maxima and bifurcation representations provides an ex-
ιent means of revealing renormalisation parameters of functions in one and
ι dimensions. In particular, the inverse problem of the recovery of invariant
nsformations is shown to be feasible. The results presented should be con-
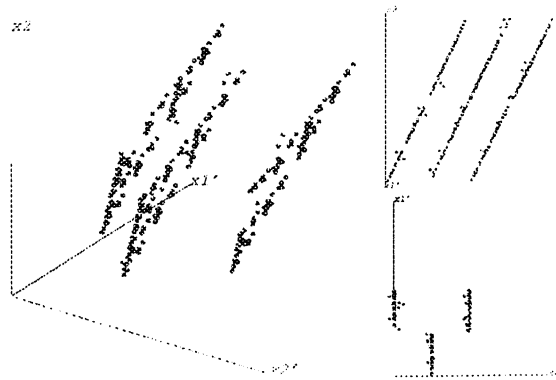ered as a first step in the direction of the general approach - application of

FIGURE 29. The maps recovered from matching the bifurcations in the representation in figure 2. Of the total of six two-dimensional maps, three maps $x_2 = f(x_1', x_2')$ are shown in the leftmost figure. The Sierpiński triangle was rotated in order to disconnect the maps. The projection along x_1' in the upper right shows consistent slope of $1/\sigma_n = 1/0.5$ rate with respect to x_2' for all three maps displayed. As expected from the diagonal S_{x_n} for the Sierpiński triangle, the linear dependence shows in only one of the coordinates, which is confirmed in the projection in the bottom right figure.
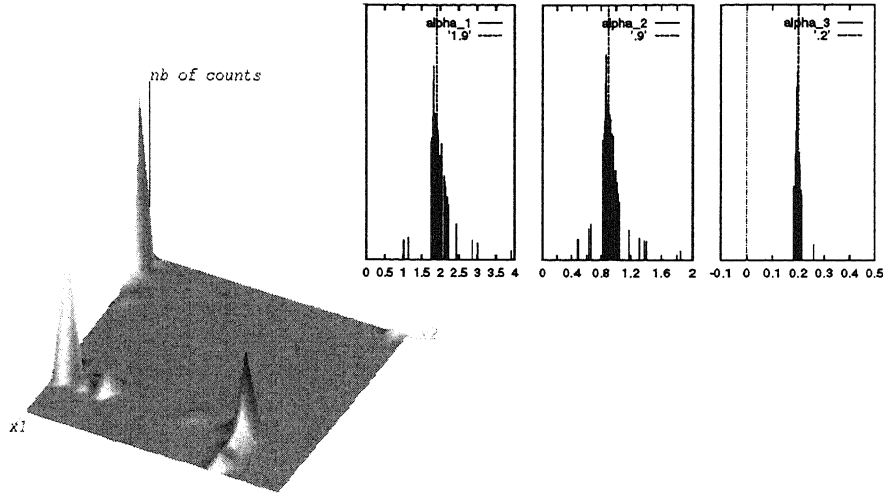

FIGURE 30. The histogram of the parameters e_n and f_n shows the location of the peaks on a triangle corresponding with the translation vectors of the Sierpiński triangle (left). The modes of the parameter α_n responsible for the distribution of the measure on the triangle (right) show remarkable agreement with the true values.

150

the scheme to real-life examples will certainly bring serious challenges.

REFERENCES

1. B.B. MANDELBROT (1982). *The Fractal Geometry of Nature*, W.H. Freeman, N.Y.

2. M.F. BARNSLEY (1988). *Fractals Everywhere*, Academic Press, NY.

3. Z.R. STRUZIK, E.H. DOOIJES, F.C.A. GROEN (1995). The Solution of the Inverse Fractal Problem with the Help of the Wavelet Decomposition, in *Fractal Reviews in the Natural and Applied Sciences*, M. M. Novak (ed.), Chapman & Hall, London.

4. Z.R. STRUZIK (1996). From Coastline Length to Inverse Fractal Problem: The Concept of Fractal Metrology, *Thesis*, University of Amsterdam.

5. A. ARNEODO, G. GRASSEAU, M. HOLSCHNEIDER (1988). Wavelet Transform on Multifractals, *Physical Review Letters* **61**, 2281–2284.

6. A. ARNEODO, E. BACRY, J.F. MUZY (1996). The Thermodynamics of Fractals Revisited with Wavelets, *Physica A*, **213**, 232–275.

7. A. ARNEODO, E. BACRY, S. JAFFARD, J.F. MUZY (1996). *Oscillating Singularities on Cantor Sets: A grand-canonical multifractal formalims*, preprint, .

8. Z.R. STRUZIK (1995). The Wavelet Transform in The Solution to the Inverse Fractal Problem, *Fractals* **3** No.2, 329–350 .

9. Z.R. STRUZIK (1996). Solving the Two-Dimensional Inverse Fractal Problem with the Wavelet Transform, *Fractals* **4**.

10. K. FALCONER (1990). *Fractal Geometry - Mathematical* FOUNDATIONS AND APPLICATIONS, John Wiley.

11. M.M. ABBOTT, H.C. VAN NESS (1972). *Thermodynamics*, Schaum's Outline Series, McGraw-Hill.

12. I. DAUBECHIES (1992). *Ten Lectures on Wavelets*, S.I.A.M.

13. S.G. MALLAT, S. ZHONG (1992). Complete Signal Representation with Multiscale Edges, *IEEE Trans. PAMI* **14**, 710–732.

14. J.S. GERONIMO, D. HARDIN, Fractal Interpolation Surfaces and Related 2-D Multiresolution Analysis, *J. Math. Anal. and Appl.* **176**, 561–586.